UNCLASSIFIED

AD NUMBER

ADB029162

NEW LIMITATION CHANGE

TO

Approved for public release, distribution unlimited

FROM

Distribution authorized to U.S. Gov't. agencies only; Test and Evaluation; 01 MAY 1978. Other requests shall be referred to Air Force Flight Dynamics Lab., Wright-Patterson AFB, OH 45433.

AUTHORITY

WL/DORT ltr, 1 Feb 1966

THIS PAGE IS UNCLASSIFIED

(18) AFFDL-TR-78-50-VOL-1
Volume I

(19)

(2) LEVEL

AD B029162

VOL. B-1 330L

(6)

FASTOP-3: A STRENGTH, DEFLECTION, AND FLUTTER OPTIMIZATION PROGRAM FOR METALLIC AND COMPOSITE STRUCTURES

Volume I -- Theory and Application

GRUMMAN AEROSPACE CORPORATION
BETHPAGE, NEW YORK 11714

(11) MAY 78 (12) 93 p.

(10) Joel Markowitz Gabriel Isakson

TECHNICAL REPORT AFFDL-TR-78-50, Volume I
Final Report, [redacted] May 77 — May 78

(7) (15) F33615-77-C-3027 (16) 2401 (17) 02

AIR FORCE FLIGHT DYNAMICS LABORATORY
AIR FORCE WRIGHT AERONAUTICAL LABORATORIES
AIR FORCE SYSTEMS COMMAND
WRIGHT-PATTERSON AIR FORCE BASE, OHIO 45433

NOTICE

When Government drawings, specifications, or other data are used for any purpose other than in connection with a definitely related Government procurement operation, the United States Government thereby incurs no responsibility nor any obligation whatsoever; and the fact that the government may have formulated, furnished, or in any way supplied the said drawings, specifications, or other data, is not to be regarded by implication or otherwise as in any manner licensing the holder or any other person or corporation, or conveying any rights or permission to manufacture, use, or sell any patented invention that may in any way be related thereto.

This technical report has been reviewed and is approved for publication.

Terry M. Harris

TERRY M. HARRIS
Project Monitor
Optimization Group
Analysis & Optimization Branch

Charles A. Bair

CHARLES A. BAIR, JR., MAJOR, USAF
Chief, Analysis & Optimization Branch

FOR THE COMMANDER

Ralph L. Kuster Jr.

RALPH L. KUSTER, JR., COLONEL, USAF
Chief, Structural Mechanics Division

"If your address has changed, if you wish to be removed from our mailing list, or if the addressee is no longer employed by your organization, please notify AFFDL/FBR, W-P AFB, OH 45433 to help us maintain a current mailing list".

Copies of this report should not be returned unless return is required by security consideration, contractual obligations, or notice on a specific document.

AIR FORCE/56780/29 June 1978 — 150

SECURITY CLASSIFICATION OF THIS PAGE (When Data Entered)

REPORT DOCUMENTATION PAGE

READ INSTRUCTIONS BEFORE COMPLETING FORM

1 REPORT NUMBER: AFFDL-TR-78-50, Volume I	2 GOVT ACCESSION NO
3 RECIPIENT'S CATALOG NUMBER	
4 TITLE (and Subtitle): FASTOP-3: A STRENGTH, DEFLECTION AND FLUTTER OPTIMIZATION PROGRAM FOR METALLIC AND COMPOSITE STRUCTURES. Volume I - Theory and Application	5 TYPE OF REPORT & PERIOD COVERED: Final Report, May 1977 - May 1978
	6 PERFORMING ORG. REPORT NUMBER
7 AUTHOR(s): Joel Markowitz and Gabriel Isakson	8 CONTRACT OR GRANT NUMBER(s): F33615-77-C-3027
9 PERFORMING ORGANIZATION NAME AND ADDRESS: Grumman Aerospace Corporation, Bethpage, New York 11714	10 PROGRAM ELEMENT, PROJECT, TASK AREA & WORK UNIT NUMBERS: Program Element: 62201F; Project: 2401; Task: 240102; Work Unit: 24010204
11 CONTROLLING OFFICE NAME AND ADDRESS: Air Force Flight Dynamics Laboratory, Air Force Wright Aeronautical Laboratories, Air Force Systems Command, Wright-Patterson Air Force Base, Ohio 45433	12 REPORT DATE: May 1978
	13 NUMBER OF PAGES: 82
14 MONITORING AGENCY NAME & ADDRESS (if different from Controlling Office)	15 SECURITY CLASS. (of this report): Unclassified
	15a DECLASSIFICATION/DOWNGRADING SCHEDULE

16 DISTRIBUTION STATEMENT (of this Report)

Distribution limited to U.S. Government agencies only; test and evaluation; statement applied 1 May 1978. Other requests for this document must be referred to AF Flight Dynamics Laboratory, FBR, Wright-Patterson AFB, Ohio 45433.

17 DISTRIBUTION STATEMENT (of the abstract entered in Block 20, if different from Report)

18 SUPPLEMENTARY NOTES

19 KEY WORDS (Continue on reverse side if necessary and identify by block number)

Structural Analysis
Flutter Analysis
Structural Optimization
Flutter Optimization
Minimum-Weight Design

20 ABSTRACT (Continue on reverse side if necessary and identify by block number)

This report presents the results of an effort to improve the usefulness of the FASTOP (Flutter And STrength Optimization Program) computer-program system, originally documented in AFFDL-TR-75-137, by introducing the capabilities of the ASOP-3 program, as documented in AFFDL-TR-76-157. The new version of the system is named FASTOP-3.

(over)

DD FORM 1 JAN 73 1473 EDITION OF 1 NOV 65 IS OBSOLETE

SECURITY CLASSIFICATION OF THIS PAGE (When Data Entered)

78 08 07 034

20 ABSTRACT (Continued)

The following improvements have been made:

1. Composite materials of laminated filamentary construction can be resized for strength and flutter-speed constraints with the same level of automation that previously existed for metallic construction.

2. A deflection constraint generalized as a linear combination of translational displacements at several structural nodes can be applied to metallic and composite structures. This permits the treatment of constraints on lifting-surface twist and camber.

3. Multiple deflection constraints can be treated in a limited, but practically important, class of problems by multiple submissions of single-constraint cases. This process has been largely automated.

4. Elastic restraint at structural support points can be treated.

5. Reactions at rigid and elastic supports are computed and their resultants determined.

This report is presented in two volumes:

Volume I - Theory and Application.

Volume II - Program User's Manual.

FOREWORD

This final report was prepared by the Structural Mechanics Section of the Grumman Aerospace Corporation, Bethpage, New York, for the Structural Mechanics Division, Air Force Flight Dynamics Laboratory, Wright-Patterson Air Force Base, Ohio. The work was performed under Contract No. F33615-77-C-3027, which was initiated under Project No. 2401, "Structural Mechanics", Task No. 02, "Design and Analysis Methods for Aerospace Vehicle Structures". Initially Mr. R. F. Taylor (FBR) was the AFFDL engineer for this contract, after which Mr. T. M. Harris (FBR) assumed the position.

The report consists of two volumes. Volume I, entitled "Theory and Application", describes the analysis and redesign procedures used in a computer program system (FASTOP-3) for minimum-weight design of metallic and composite lifting-surface structures subjected to combined strength and flutter-speed requirements or combined strength and deflection requirements. Emphasis is placed on capabilities that are new in FASTOP-3 compared with earlier versions of the FASTOP system. Detailed instructions on the use of the FASTOP-3 system are provided in Volume II, entitled "Program User's Manual". The report, which covers work conducted between 1 May 1977 and 1 May 1978, was submitted to the Air Force in May 1978.

Drs. J. Markowitz and G. Isakson were the Project Engineers. The authors gratefully acknowledge the suggestions and advice of Messrs. E. Lerner and J. Smedfjeld and Dr. W. Lansing. They are also indebted to Messrs. D. George and P. Stylianos for assistance on programming aspects, and to Mr. G. Schriro for assistance with report preparation.

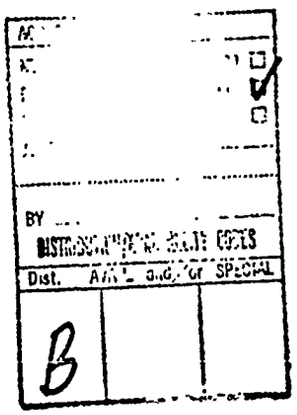

TABLE OF CONTENTS

TABLE OF CONTENTS (concluded)

LIST OF ILLUSTRATIONS

LIST OF ILLUSTRATIONS (Continued)

LIST OF TABLES

Section 1

INTRODUCTION

In December 1975, Grumman, under contract to the Air Force Flight Dynamics Laboratory, completed development of a large scale computer program system named FASTOP (Flutter And STrength Optimization Program) which is capable of performing integrated interdisciplinary analysis and redesign for aircraft lifting-surface structures (Reference 1). That program, henceforth referred to as FASTOP-1, can analyze designs with respect to loads, strength, vibration and flutter, but most importantly, the program is also capable of obtaining near-optimum designs for lifting-surface structures subjected to both strength and flutter-speed requirements.

The strength analysis and optimization module of FASTOP-1 is based, with some modifications, on a version of ASOP (Automated Structural Optimization Program) that had been developed for the Air Force several years earlier (Reference 2). That version, now known as ASOP-1, is limited to noncomposite materials. Accordingly, FASTOP-1 cannot be used for interactive strength/flutter resizing of composite structures; it can be used for flutter resizing alone, but the associated input data requirements are rather cumbersome.

The ASOP-1 program was followed by the development of two successively more sophisticated versions, ASOP-2 and ASOP-3, each of which have increased capability for treating composite materials (References 3 and 4). Among other improvements, ASOP-2 is able to perform strength resizing of laminated filamentary composites of 0°/90°/±45° balanced layup. The most recent version, ASOP-3, treats composites in a rather comprehensive manner. Specifically, it can accommodate laminates with up to six arbitrary fiber directions, enforce "balanced" laminate requirements if desired, and apply practical design criteria during resizing. Moreover, the program has an improved algorithm for interactive strength/deflection resizing which follows closely the procedure for strength/ flutter resizing in FASTOP-1.

In view of the ASOP-3 program's extensive capabilities with respect to the treatment of composites, an effort was undertaken to introduce those capabilities into the FASTOP system. Two major tasks were accomplished.

First, all of the features of ASOP-3 were incorporated, with no loss of capability, into the strength analysis and optimization module of FASTOP-1. Second, the flutter optimization module of FASTOP-1, as well as all of the subroutines associated with interactive strength/flutter resizing, were modified to accommodate composites. The new version of FASTOP, designated FASTOP-3, is described in the present report.*

Several useful features, not present in either FASTOP-1 or ASOP-3, have also been introduced into FASTOP-3. These include the computation of reactions at rigid and flexible support points, and an automated restart capability for deflection resizing which greatly facilitates the treatment of multiple deflection constraints by means of successive applications of the program.

This report has been written as a supplement to the original FASTOP report (Reference 1) and is not intended to serve as a stand-alone document. Where FASTOP has changed little, or not at all, the program description is kept very brief, and it is expected that a reader new to FASTOP will read the pertinent portions of Reference 1. Where extensive changes have been made, as in resizing for strength and deflection constraints, the description is sufficiently complete that the reader can gain a good understanding of the principal features of the process. However, for some details on strength and deflection resizing the interested reader should refer to Reference 4.

The major unique capability of FASTOP-3, namely interactive strength/flutter resizing of composite lifting-surface structures, has been demonstrated on two sample structures. Results of the two redesign studies are presented in some detail. Also, in order to verify that the ASOP-3 capabilities have been incorporated successfully into FASTOP-3, it was necessary to apply FASTOP-3 to a strength/deflection redesign problem that had been addressed previously by ASOP-3. The results obtained for this additional redesign problem, using FASTOP-3, are included in this report.

*The designation FASTOP-2 pertains to a modified version of FASTOP-1 developed by the University of Dayton and used by personnel at the Air Force Flight Dynamics Laboratory.

Section 2

MODIFICATIONS TO THE ORIGINAL FASTOP SYSTEM

This section contains descriptions of the theory and procedures associated with the analysis and redesign capabilities of FASTOP-3. The focus is on the differences between FASTOP-3 and the original version of the program. Where these differences are small, or nonexistent, the discussion is very brief and the reader is referred to the proper section of the original FASTOP theory report (Reference 1). Where the differences are extensive, namely in the area of strength/deflection analysis and redesign, the discussion is quite thorough and it is hoped that the material is sufficient for the reader to grasp the important concepts and procedures. For related details, however, the reader should consult the ASOP-3 final report (Reference 4).

The following subsections are arranged so as to correspond with the order in which topics are presented in Reference 1.

2.1 OVERVIEW OF THE FASTOP SYSTEM

The FASTOP system is divided into two major programs, the first of which addresses static analysis and redesign functions, and the second of which addresses aspects of dynamic analysis and redesign. Each of these two programs, namely the Strength Optimization Program (SOP) and the Flutter Optimization Program (FOP), is further divided into a number of special purpose modules. For FASTOP-3, the capabilities of some of these modules have changed. Accordingly, the new capabilities of all the various analysis and redesign modules are summarized below:

Applied Loads

- Aerodynamic
  - Maximum number of flight conditions 20
  - Maximum number of aerodynamic panels
    - o Subsonic 150
    - o Supersonic 100
  - Maximum number of control surfaces 8

- Inertial
  - Maximum number of flight conditions 20
  - Maximum number of distributed (point) masses 1000
  - Maximum number of concentrated (mass and inertia) masses 100

Strength and Deflection Analysis and Resizing

- Analysis
  - Maximum allowable number of finite elements to define the structure's model 3000
  - Maximum number of structures-model node points 1000
  - Maximum number of structures-model degrees of freedom 6000*
  - Maximum number of applied load conditions 20
- Resizing
  - Maximum number of variables for resizing
    - o strength 10000
    - o deflection 6000

Vibration Analysis

- Applicable to cantilever or free-free structures
  - Maximum number of dynamics-model degrees of freedom 200

Flutter Analysis

- Assumed-pressure-function and doublet-lattice routines for subsonic flow M=0 → 0.9
- Mach-box routine for supersonic flow M=1.2 → 3.0
- Maximum number of modes for flutter analysis 20
- Maximum number of control surfaces on main surface for doublet-lattice and Mach-box routines 5
- Maximum number of aerodynamic panels
  - o doublet-lattice 400
  - o Mach-box 350

*Reduces to 3000 if subsequent flutter resizing uses a free-free vibration model; unchanged for cantilever model.

Flutter Resizing

- Maximum number of variables which can be resized for flutter
  - o structural variables 6000*
  - o mass-balance variables 20

A comprehensive review of the FASTOP system is contained in Section 2 of Reference 1.

2.2 APPLIED LOADS ANALYSIS

The computation of applied loads in FASTOP-3 differs from that of the original version only in that the maximum number of load conditions has been increased to 20. Both aerodynamic and inertial loads can be generated, each type being computed with respect to its own math model. The two sets of loads are then transformed to the structures model (by means of transformation matrices discussed elsewhere) for use in structural analysis. Computation of the aerodynamic-influence-coefficient matrices is based on either subsonic vortex-lattice theory or supersonic source-distribution theory. For the latter, two general flow conditions are considered, namely supersonic leading and trailing edges, and subsonic leading and supersonic trailing edges. Details of the applied loads analysis are presented in Section 3 of Reference 1.

2.3 STRENGTH AND DEFLECTION ANALYSIS AND RESIZING

2.3.1 Summary

The strength and deflection analysis and resizing capability of the ASOP-3 program (Reference 4) has been incorporated into the SOP program, replacing the earlier version of ASOP previously used in FASTOP. This change greatly enhances the utility of the SOP program, as follows:

*Reduces to 4800 if maximum allowable sizes have been prescribed for any of the structural variables involved in the flutter resizing process.

(1) Composite materials of laminated filamentary construction can be treated explicitly and efficiently. In any composite element, the number of laminae in each group of laminae of a given material, and having a common fiber orientation, is treated as a separate design variable.

(2) The program can resize to satisfy strength constraints and a single deflection constraint interactively. The deflection that is to be constrained can be generalized in the sense that it can be expressed as a linear combination of translational displacements at selected nodes. However, the constraint can be applied in only a single load condition. Multiple deflection constraints can be treated in a limited class of problems by multiple passes through the program, within each of which a single deflection constraint is applied.

(3) Up to twenty load conditions can be accommodated in resizing for strength.

2.3.2 Finite-Element Modeling

The available finite elements are the same as in the ASOP-3 program. They consist of a uniform-cross-section bar element (type 1), two prismatic beam elements (types 2 and 11), a triangular membrane element (type 4), two quadrilateral membrane elements (types 5 and 8), and a quadrilateral shear panel (type 6). In contrast with the original version of FASTOP, all of the membrane elements (types 4, 5, and 8) can be of composite construction, and the type-2 uniform beam element has been generalized to provide for offset of the element nodes from the beam centroidal axis. The plate bending elements (types 15 and 16) and combined membrane and plate bending elements (types 17 and 18) are not available in the new program.

Composite elements can have up to six layers, where a "layer" is defined as the aggregate of all laminae of a given composite material (for example, graphite/epoxy), and with fibers in a given direction. The fiber directions for the different layers can be arbitrary, except that, in aggregate, the layers should constitute a laminate whose strength is filament-controlled (as defined in Subsection 2.3.4.3). It should be noted that the laminae in a

layer, as defined above, will not normally be contiguous in an actual laminate, but, in membrane action, their combined effect will be the same as if they were contiguous.

A composite material, as defined in the program for the purpose of data input, consists of the whole laminate, including numbers of layers, filament direction in each layer (relative to the x_p-axis in the property axis system), and properties of the material in each layer. Starting and, if desired, minimum and maximum numbers of laminae in each layer are also specified.

Layers of composite elements are treated internally in the program as separate elements, except in resizing for stress constraints, where the interaction between them is accounted for, as discussed in Subsection 2.3.4.3. The layers of a composite element thus constitute a stack of elements that are connected at the corner nodes only. In the case of quadrilateral elements, which consist of an assemblage of triangular elements with a common interior node, there may be some relative displacement of these interior nodes among layers in a laminate. This effect is believed to be small, however, and should not introduce any significant error.

In the specification of material properties, three different classes of materials are distinguished: isotropic, orthotropic, and composite, with composite materials defined as discussed above. If the elastic properties of a member are more generally anistropic, they may still be introduced, but the necessary data must then be entered through member data cards. (The members are the finite elements of the structural model, and the terms "member" and "finite element" or "element" are used here interchangeably.) The member data specify the element type, the material code, the nodes it connects, and other required geometrical data and program clues. In addition, material stiffness and strength data may be specified, if desired, with the member data, rather than through the material property data, as explained in Volume II of this report. Likewise, in the case of composite members, the layer properties may be introduced on member data cards, instead of through the material properties input.

For one-dimensional members or elements (bars and beams), a single system of orthogonal coordinate axes suffices. In the case of two-dimensional elements, however, at least two systems of orthogonal axes are used, as shown in Figure 2.1 for a quadrilateral element. One of these, named the

"local element axes," x_ℓ, y_ℓ, z_ℓ, is oriented so that the origin is at node i, where the nodes are entered in the program in the order i, j, k, ℓ, and are arranged as shown in Figure 2.1. The x_ℓ-axis is along the edge i-j, positive toward j; the y_ℓ-axis is positive toward the side on which the element lies; and the z_ℓ-axis completes a right-handed triad. While the direction i to j is shown as being counterclockwise around the element in Figure 2.1, it can just as well be clockwise, as long as node k is on a common edge with node i, and node ℓ with node j. For planar elements, the local element axes are in the plane of the element, while in the case of warped quadrilateral elements, they are in a plane defined by a pair of straight lines joining the midpoints of opposite sides, as discussed in Appendix E.2 of Reference 4.

The use of a second set of axes, the "property axes," x_p, y_p, is mandatory when the material is not isotropic. These axes, which are in the same plane as the x_ℓ and y_ℓ axes, are aligned with directions having significance in the definition of material properties. For example, in the case of orthotropic materials, they are the axes of symmetry in the material properties.

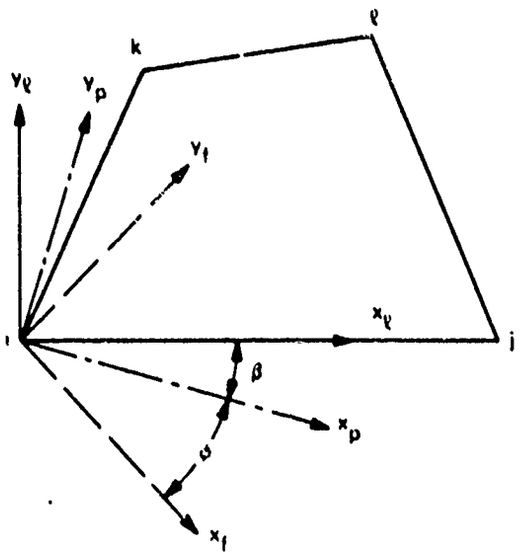

Figure 2.1 Member Axis Systems

For composite materials, they can be arbitrary, but are normally related in some simple manner to the fiber directions, as, for example, in the case of a 0°/90°/±45° laminate, where a natural choice for the x_p-axis would be the 0° direction. It is necessary to define property axes, even for isotropic elements, when the user desires that the stress and strain output not be referred to the local element axes. The property axes then define the axes to which the stresses and strains are to be referred.

The angle between the x_ℓ and x_p axes is referred to as the "β-angle," and is positive as shown in Figure 2.1, that is, when a rotation from x_ℓ to x_p is away from the element, rather than into the element. There are two ways of specifying this angle for each member. One way is to enter it directly with the data for each member, but this requires that it be precalculated for all the members - a task that can be formidable. The other way is to separate the members into groups or "zones", and have the program automatically compute the β-angles for all the members in each zone on the basis of a "reference direction" defined for that zone. The β-angle is the angle between the projection of the reference direction in the plane of the member (or the i-j-k plane in the case of warped elements) and the x_ℓ-axis. The relations used in that calculation are presented in Appendix C of Reference 4. Only the zone number need then be specified for each member, the reference direction being defined elsewhere for each zone.

In the case of composite members, there is a third set of orthogonal axes defined for each layer. These axes are the "fiber axes," x_f, y_f, which are in the same plane as the x_p and y_p axes (and also the x_ℓ and y_ℓ axes) and are aligned so that the x_f-axis is in the fiber direction. The angle between the x_f and x_p axes is the angle ϕ defined for each layer in the input for the composite material. It is positive in the same sense as β, that is, when a rotation from x_p to x_f is away from the element, as shown in Figure 2.1.

While the various systems of axes have been defined above with reference to quadrilateral elements, the definitions remain the same for triangular elements.

2.3.3 Analysis Procedure

The analysis procedure is essentially the same as in the original version of FASTOP. That is, it applies the matrix displacement method, stacking the element stiffness matrices to form a structure stiffness matrix, with due

account taken of boundary conditions. The matrix equation relating applied loads to nodal deflections, through the structure stiffness matrix, is then solved for the nodal deflections, which are subsequently used to determine corner forces acting on the individual elements.

As discussed in Subsection 2.3.2, the layers of a composite element are treated as separate elements in the stacking process. In determining their stiffness matrices for this purpose, the full stiffness properties of the lamina material, including the matrix material, are taken into account. This differs from the procedure in the resizing process, where the stiffness of the matrix material is neglected in determining layer stresses.

A new capability introduced into the program involves the calculation of the support reactions. The force and moment resultants of all the reactions for each load condition are determined, and can then be compared with the corresponding resultants of the applied loads. This provides a check of the degree to which equilibrium conditions are satisfied, and, consequently, a check of the numerical precision achieved in the analysis.

The load-displacement relations may be expressed in the matrix form,

$$\left\{\begin{array}{c} P \\ \hline R \end{array}\right\} = \left[\begin{array}{c|c} K_{11} & K_{12} \\ \hline K_{21} & K_{22} \end{array}\right] \left\{\begin{array}{c} \delta \\ \hline 0 \end{array}\right\} \qquad (2.1)$$

where $\{\delta\}$ is the vector of unconstrained nodal deflections, $\{P\}$ is the vector of applied loads in corresponding degrees of freedom, $\{R\}$ is the vector of support reactions, $\{0\}$ is a null vector, and the stiffness matrix is partitioned in a consistent manner. Thus,

$$\{P\} = [K_{11}]\{\delta\} \qquad (2.2)$$

$$\{R\} = [K_{21}]\{\delta\} \qquad (2.3)$$

Equation (2.2) is solved for $\{\delta\}$, which is then substituted into Equation (2.3) to yield the support reactions. As in the original version of FASTOP, Equation (2.2) is solved by employing the Cholesky algorithm for decomposition of positive-definite symmetric matrices (see Reference 1).

2.3.4 The Stress-Constraint Mode

2.3.4.1 Basic Procedure and Element Stress Determination

Two different phases, or "modes", in the redesign process are distinguished. In the "stress-constraint mode," a number of cycles of analysis and resizing for stress and minimum- and/or maximum-gage constraints are performed, until a convergence criterion is satisfied or the number of cycles has reached a specified maximum. The design should then be fully stressed or nearly fully stressed. If deflection-constraint resizing is not to be done, the process is completed. If deflection-constraint resizing is to be done, there is a subsequent mode, referred to as the "deflection-constraint mode," in which stress-constraint resizing and deflection-constraint resizing are done interactively, and in which minimum- and/or maximum-gage constraints may also be applied. It should be noted that minimum gages usually represent limitations associated with practical construction, while the maximum gage is normally used as a means of fixing an element's gage when the minimum and maximum gages are set equal to one another.

The basic procedure for resizing based on allowable stresses and member gage limitations is essentially the same as in the original version of FASTOP. The stiffness matrix of each finite element in the structural model is assumed to be linearly related to a single design variable for that element (bar cross-sectional area, skin gage, etc.). In the case of the beam elements, it is assumed that the radii of gyration of the cross section remain constant during resizing, so that the moments of inertia of the cross section, and consequently the bending stiffness, are proportional to the cross-sectional area, which is the design variable in this case.

An initial design, specifying values of the design variables, is selected, and an analysis to determine nodal deflections and element stresses is carried out, for a given set of applied loading conditions. The state of stress in each element, for each loading condition, is then used in conjunction with a failure criterion to determine a "stress ratio". This ratio provides a measure of the extent to which the stress constraint is satisfied or violated, and is discussed in detail in Subsections 2.3.4.2 and 2.3.4.3. It is equal to 1.0 if the failure criterion is satisfied exactly. The maximum value of the stress ratio, for all loading conditions for each element, is then used as a multi-

plying factor in resizing the design variable for that element. The procedure is considerably more complicated in the case of composite elements, as explained in Subsection 2.3.4.3.

This process of analysis and redesign is repeated cyclically, until a specified number of cycles have been performed, or until a convergence criterion is satisfied. A converged design is referred to as a fully stressed design; that is, a design in which each element is either stressed to the maximum allowable extent in at least one loading condition (without being overstressed in any loading condition), or is at a minimum or maximum prescribed gage.

The nodal stress method for element stress determination, which was used in the original version of FASTOP, has been found to have shortcomings, and has been replaced in FASTOP-3. Average stresses are now determined for an element directly from the nodal forces acting on that element. In the case of the bar element, which is a uniform-strain element, the stress is simply the quotient of the nodal force (which is the uniform axial load in the bar) and the cross-sectional area of the bar. The triangular membrane element is similarly based on the assumption of uniform strain, and the average stress in it is simply the uniform stress associated with the uniform strain. The matrix transformation relation between average stress and the corner forces in that element is derived in Appendix E of Reference 4.

The determination of average stress in the quadrilateral membrane elements (types 5 and 8) is not as straightforward, as these elements are constructed of four uniform-strain triangular elements, within each of which the strain is generally different. There are a variety of ways, necessarily approximate in nature, in which average stress can be defined in such an element. The definition used in FASTOP-3 is based on equilibrium considerations. A derivation of the applicable relations is presented in Appendix E of Reference 4. The average shear stress in the shear panel (element type 6) is determined in the same way.

In the beam elements (types 2 and 11), the axial load and corresponding stress are determined in the same way as in the bar element. Bending moments, however, are determined separately at each end of the element, and, because it is assumed that the element is loaded only at its ends, the maximum bending moment occurs at one of the ends. The shear force and torsional moment, both uniform along the element, are also determined.

2.3.4.2 Resizing Algorithm for Noncomposite Elements

The resizing of bar elements is particularly simple because of the uniaxial stress state in them, the stress ratio being the ratio of the actual stress to the allowable stress. In the resizing of beam elements, it is assumed that the element is loaded in bending primarily about only one of the two transverse axes: the z-axis. The bending moment about that axis is then determined at the two ends of the element, and corresponding extreme-fiber stresses are determined at the two ends, assuming that the distance of the extreme fiber from the neutral axis is equal to the radius of gyration of the cross section (which, in effect, assumes that the bending material is concentrated at the extreme fiber). The bending stresses are then combined with the stress due to the axial load, yielding four values of stress - two extreme-fiber stresses at each end of the element - and corresponding stress ratios are determined. The largest of these stress ratios is then selected for resizing purposes.

The biaxial stress state in membrane elements requires that a failure criterion, providing for the interaction between stress components, be used. In the case of isotropic materials, it is common to use the von Mises yield criterion, with ultimate allowable stresses usually replacing the yield stresses, and that criterion is used in FASTOP-3, in the following modified form:

$$\sqrt{\left(\frac{\sigma_x}{F_x}\right)^2 - \left(\frac{\sigma_x}{F_x}\frac{\sigma_y}{F_y}\right) + \left(\frac{\sigma_y}{F_y}\right)^2 + \left(\frac{\tau_{xy}}{F_s}\right)^2} = 1 \qquad (2.4)$$

where F_x is either the allowable tensile stress F_t or the allowable compressive stress F_c, depending upon the sign of σ_x; F_y is either F_t or F_c, depending upon the sign of σ_y; and F_s is the allowable shear stress. F_t, F_c and F_s are always taken as positive quantities. The stress ratio in this case is the left-hand side of Equation (2.4).

In the case of orthotropic materials, the picture is less clear and there is no universally accepted failure criterion. Two relatively simple criteria, having a somewhat rational basis, are Hill's generalization of the von Mises criterion and a criterion developed originally at the Forest Products Laboratory (References 5 and 6). In the absence of conclusive experimental evidence favoring either one of these criteria, the latter was selected for use in ASOP-3, and is used also in FASTOP-3.

It is expressed in the form:

$$\sqrt{\left(\frac{\sigma_x}{F_x}\right)^2 - \left(\frac{\sigma_x}{F_x}\frac{\sigma_y}{F_y}\right) + \left(\frac{\sigma_y}{F_y}\right)^2 + \left(\frac{\tau_{xy}}{F_s}\right)^2} = 1$$

$$\frac{\sigma_x}{F_x} = 1 \qquad (2.5)$$

$$\frac{\sigma_y}{F_y} = 1$$

where σ_x, σ_y and τ_{xy} are the stress components in the property axis system; F_x, F_y and F_s are the corresponding allowable stresses in the absence of the other components; and failure is presumed to occur when any one of the three relations is satisfied. F_x and F_y are tensile or compressive allowable stresses, as appropriate, and are always taken as positive quantities.

In applying this criterion, the left-hand sides of all three relations are evaluated, and the largest of the three becomes the governing stress ratio, which is then used as a multiplying factor in resizing, as described in Subsection 2.3.4.1.

The failure criterion expressed by Equation (2.5) is shown graphically as an envelope, in Figure 2.2, for the case, $\tau_{xy} = 0$. The first of the equations is represented by the ellipse, and the remaining two equations effectively apply cutoffs in the first and third quadrants. It can be seen that the ellipse, in Figure 2.2, also represents Equation (2.4), which is the failure criterion for isotropic materials. If desired, the cutoffs shown in Figure 2.2 can be applied to isotropic materials as well, by suitable adjustment of the input data, as explained in Volume II of this report.

The new element gages obtained in this way are checked against the minimum gages specified in the input data, and are revised accordingly, if necessary. If the stress resizing is being done as part of a cycle in the deflection-constraint mode, as discussed in Subsection 2.3.4.2, a similar check is made against the minimum gages established by deflection-constraint resizing, and necessary revisions are made. Similarly, if the stress resizing is being done subsequent to flutter resizing, the flutter-governed gages are now treated as minimum gages. A check is then made against the maximum gages specified in the input data, and necessary revisions are made.

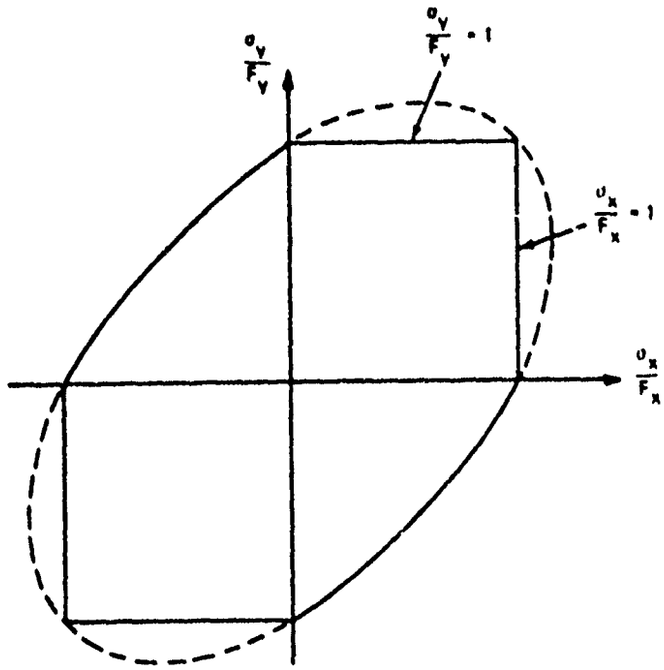

Figure 2.2 Failure Criterion for Orthotropic Materials in Biaxial Stress

While composite elements can (it is expected that they usually will) be resized by the comprehensive procedure described in the following section, a cruder approach can be used, in which they are treated as orthotropic elements and resized by the procedure described above. In that case, it is necessary that the layup be such that the relative numbers of laminae in the various fiber directions are maintained constant, so that appropriate allowable stresses can be selected. It will be seen that the cutoffs described in the following section bear some similarity to those shown in Figure 2.2.

2.3.4.3 Resizing Algorithm for Composite Elements

The criteria governing the failure of composites are more complex than those governing the failure of noncomposite materials. In consequence, the algorithm for composite element resizing is necessarily more complex, requiring that the laminate be treated as a unit, so that interaction between layers may be properly taken into account. Furthermore, because of limited operational experience with composite materials, it is desirable to make certain conservative assumptions concerning their strength behavior.

For example, local cracking or crazing in the matrix material may greatly reduce its effectiveness as a load-carrying agent, even though it continues to serve its central purpose as a binding agent. For that reason, the assumption is made here that all the load is carried by the filaments.* This assumption is applicable only to so-called filament-controlled composites: those in which the layup is such that filament directions are sufficient in number and distribution that any component of the laminate stress resultant can be resisted by filaments alone It would not be a tenable assumption in the case of matrix-controlled composites: those in which the load-carrying capability of the matrix is relied upon. The program does not, at present, accommodate composites of this latter type, although it can be further developed to do so.

Another conservatism, one that may be applied as an option in the program, relates to interaction between laminate layers that is somewhat akin to the effect of hydrostatic stress in metals or other nominally homogeneous materials It is known, for example, that, if components N_x and N_y of the laminate stress resultant are present and are of the same sign, some layers will be less severely stressed than if either N_x or N_y were absent. Some designers feel that it is unconservative to take advantage of this fact and to base the design on the simultaneous presence of both components, particularly since the prediction of applied loads is hardly an exact science, and the dynamic nature of some loading conditions suggests the possibility that different components of the internal loading may not be applied simultaneously. The program option referred to as the "cutoff option" makes it possible to provide additional stress checks, with N_x and N_y successively set to zero, and to use the results as additional information in the resizing process.

In addition to filament failure in tension or block compression, the possibility of failure in the so-called "microbuckling" mode may be taken into account. In that mode, there is a highly-localized buckling of the filaments because of their own low bending stiffness and the limited shear stiffness of the matrix material, which is relied upon to resist such buckling (Reference

*Note that, as stated in Section 2.3.3, this assumption is made only in the resizing process. In the analysis of the whole structure, to determine nodal displacements and internal loads, the full stiffness properties of the composite elements, including the contribution of the matrix material, are used.

7). Theoretically, it has been found that the allowable stress, G_z, in this mode, should be equal to $G_m/(1 - V_f)$, where G_m is the shear stiffness of the matrix material, and V_f is the volume fraction of fibers (Reference 7); however, experimental evidence indicates that it is better to use a value based on experimental data (Reference 8). If experimental data are not available, the theoretical value may be multiplied by an empirical coefficient which, at least for the case of boron/epoxy, can be given the value 0.63 (Reference 9).

To properly account for the interaction between layers, the resizing algorithm for composite elements treats the entire laminate as a unit and applies a convergent iteration procedure. This procedure is summarized in flow-chart form in Figure 2.3 and is described in detail in Reference 4. Essentially, it uses the stress resultant on the whole laminate to determine stresses in the layers (neglecting the effect of matrix stiffness), and then resizes the layers using stress ratios. Minimum/maximum constraints are then applied and the layer thickness is rounded up to the nearest multiple of the lamina thickness. The process is repeated cyclically until convergence is achieved. A microbuckling failure criterion, cutoffs (as discussed earlier), and layer 'balancing' may be applied. Balancing forces specified layers always to have the same number of laminae. It is accomplished by setting the number of laminae in all such layers equal to the number of laminae in the most severely stressed layer.

2.3.4.4 Resizing of Compression Members

The limited capability introduced into the original version of FASTOP for the resizing of bars and shear or compression panels subject to buckling failure has been retained in FASTOP-3. It involves the introduction of "stability tables" relating allowable stresses to internal loading. This capability is limited to noncomposite elements.

2.3.5 The Deflection Constraint Mode

2.3.5.1 Resizing Algorithm

It is shown in Appendix G.1 of Reference 4 that, for the case of a single deflection constraint and in the absence of other constraints, a minimum

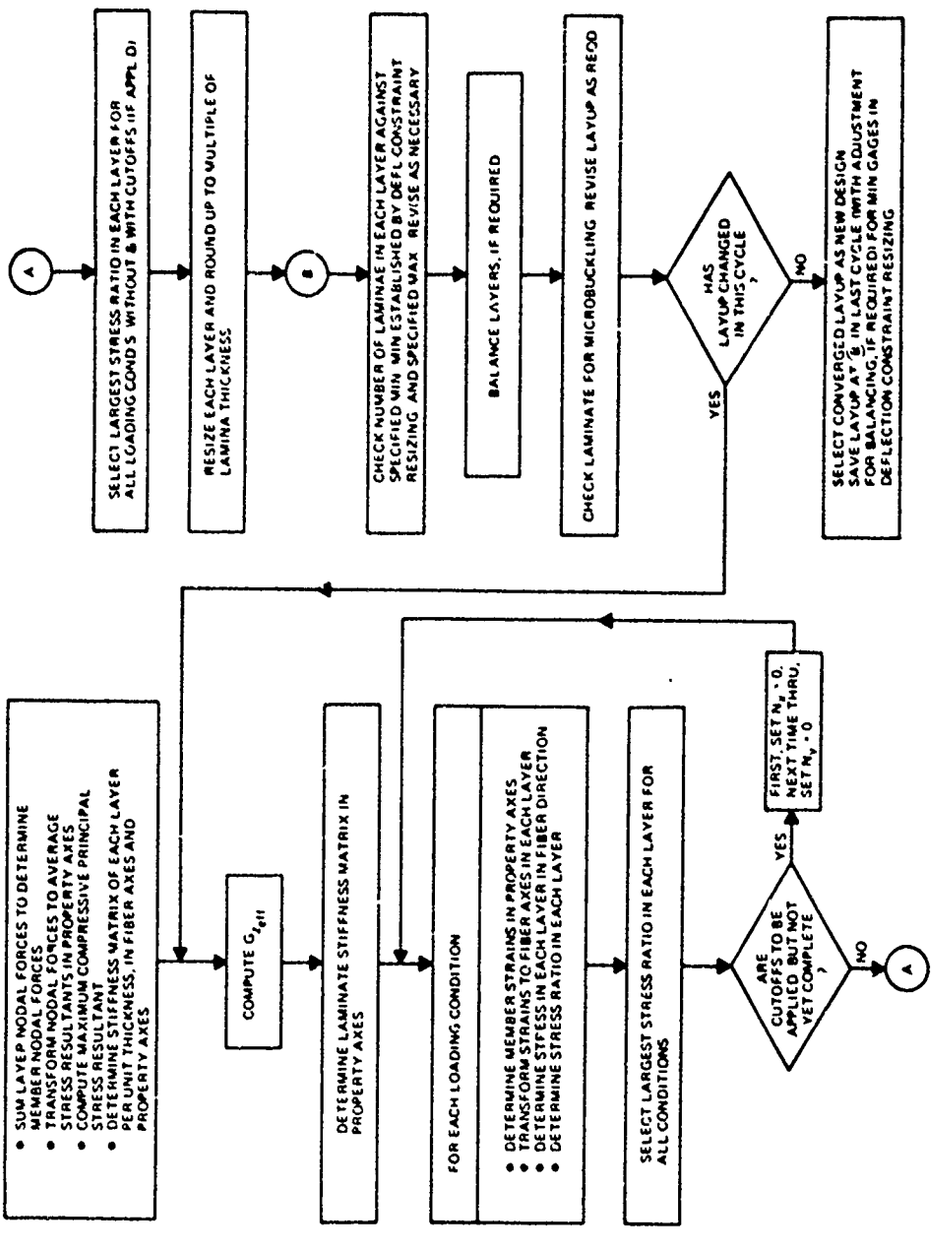

Figure 2.3 Cyclic Process for Stress-Constraint Resizing of Composite Elements

weight is achieved when the partial derivative of the constrained deflection with respect to element weight has the same value for all elements, that is, when

$$\frac{\partial \delta}{\partial w_i} = K \qquad (i = 1, 2, \ldots . n) \tag{2.6}$$

where δ is the deflection to be constrained, w_i is the weight of the i^{th} element (of a total of n elements), and K is a constant.

When, as in most practical designs, there are strength constraints and minimum or maximum gage constraints in addition to the deflection constraint, the uniform-derivative criterion, expressed in Equation (2.6), can be applied to the set of all elements not governed by these other constraints, the corresponding element weights being referred to as the "active" variables. In that case, the criterion is less rigorously applicable, but should still give a design of nearly minimum weight, as discussed in Appendix G.1 of Reference 4.

The minimum-weight design cannot be arrived at directly. It is necessary to employ an iterative process, which has been found to converge rapidly in practical cases. This process closely resembles the procedure used in the program for optimization to satisfy a constraint on flutter velocity.

Starting with a nonoptimum design, which may or may not satisfy the prescribed deflection constraint, the following recursion relation, derived in Appendix G.2 of Reference 4, is applied in successive cycles:

$$w_{i_{new}} = w_{i_{old}} \sqrt{\frac{\left(\frac{\partial \delta}{\partial w_i}\right)_{old}}{\left(\frac{\partial \delta}{\partial w}\right)_{target}}} \tag{2.7}$$

where $w_{i_{old}}$ is the weight of the i th element prior to resizing in the current cycle; $w_{i_{new}}$ is the weight of the i th element following resizing in the current cycle; $(\partial \delta / \partial w_i)_{old}$ is the partial derivative of the constrained deflection with respect to w_i, computed for the design existing prior to resizing in the current cycle; and $(\partial \delta / \partial w)_{target}$ is a quantity given the name "target derivative" and is defined below. The basis for Equation (2.7) is discussed in Appendix G of Reference 4.

At the optimum design, the target derivative will be the constant K in Equation (2.6), and the derivatives $\partial\delta/\partial w_i$ will all be equal to it. However, prior to convergence to an optimum design, the derivatives $\partial\delta/\partial w_i$ will differ from each other in value, and, in fact, may differ in sign. Depending upon the sign of the target derivative, some of these derivatives may then yield a negative value for the quantity under the radical in Equation (2.7). The corresponding elements will then have to be excluded when Equation (2.7) is applied.

As the value of K in Equation (2.6) is not known until the optimum design is achieved, it is necessary to find a value for the target derivative that, when introduced into Equation (2.7), will yield a design that satisfies the constraint, at least approximately. This is done by a trial procedure, in which a value of the target derivative is sought that will yield a design satisfying the relation:

$$\delta_{desired} = \delta_{old} + \sum_{i=1}^{n} \frac{1}{2}\left[\left(\frac{\partial\delta}{\partial w_i}\right)_{old} + \left(\frac{\partial\delta}{\partial w}\right)_{target}\right]\left(w_{i_{new}} - w_{i_{old}}\right) \quad (2.8)$$

where δ_{old} is the value of the constrained deflection prior to resizing; $\delta_{desired}$ is the desired value of the constrained deflection in a resizing step; and the summation is over all elements of the model, including those to which Equation (2.7) is not applied.

Equation (2.8) is seen to provide a second-order approximation (in the Taylor-series sense) to the desired value of the deflection. An exact value could have been obtained by a trial procedure in which a structural analysis is performed, for the design corresponding to each trial value of the target derivative, to determine the deflection subject to constraint. However, as this operation would have to be performed a number of times, for successive trial values of the target derivative, and is expensive computationally, it is highly advantageous and, in practice, satisfactory to use Equation (2.8) instead.

It was stated above that Equation (2.7) is applied to that group of elements with derivatives, $\partial\delta/\partial w_i$, that are of the same sign as the target derivative. The determination of that sign is now considered. The sign is established upon entry into the deflection-constraint mode and depends upon whether the constraint value of the subject deflection exceeds, or is less than, its current value (for the design existing upon entry into the deflection-constraint mode). If the constraint value exceeds the current value algebraically, and the constraint is either (1) an equality constraint or (2) an inequality constraint that has been violated, then an increase in deflection is desired, and the proper derivative sign is that which is associated with an increase in deflection resulting from an increase in element weight, that is, a positive sign. For those elements with negative derivatives, a reduction in element weight will move the deflection in the desired direction, and the design variables for these elements can be permitted to decrease, to the extent permitted by other constraints. (This is discussed further in Subsection 2.3.5.2.) In the reverse situation, where the constraint value is less than the current value, Equation (2.7) is applied to those elements with negative derivatives. Where the constraint is an inequality constraint and is not violated by the design existing at exit from the stress-constraint mode, no further resizing is necessary.

The sign of the target derivative will, by definition, be the same as that of the derivatives $(\partial\delta/\partial w_i)_{old}$ introduced into Equation (2.7). It remains to find a value of the target derivative that will satisfy Equation (2.8). This is done by taking, as an initial trial value, upon entry into the deflection-constraint mode, a value equal to 80% of the average of all the derivatives having the proper sign, determined as explained above. (In subsequent redesign cycles of the iterative redesign process, as explained below, the starting value of the target derivative is the last value computed in the preceding cycle.) The target derivative is then incremented until a value is achieved that satisfies Equation (2.8), within a tolerance specified by the user.

The value of $\delta_{desired}$ in Equation (2.8) is not necessarily the constraint value. It may be advantageous, in some situations, to move from the initial value of the subject deflection to the vicinity of the constraint value in a series of shorter steps, rather than in a single step. Equation (2.8) then

provides a closer approximation in each step. Furthermore, when the constraint boundary in the design space is reached by this procedure, it may be at a point considerably closer to the optimum design point. Accordingly, the program provides an option that permits the change from the initial value of the deflection to the constraint value to be made in a number of approximately equal increments, that number being selected by the user.

The deflection that is subject to constraint may be generalized in the sense that it may be represented as a linear combination of nodal displacements in specified degrees of freedom. Thus, for example, an angular displacement constraint may be treated by representing it as the difference between the translational displacements of two specified points, divided by the distance between them. The two points specified need not be at nodes; their displacements can be obtained by interpolation between nodal displacements. Similarly, a given amount of camber of a lifting surface, at a given spanwise station, can be specified as a constraint by a similar representation as a linear combination of nodal displacements.

When composite elements are included in the model, each layer of such elements is treated internally in the program as a separate element. Accordingly, Equation (2.7) is applied to individual layers, with the deflection derivative being computed for each layer with respect to that layer's weight. However, the derivatives of layers that are to be balanced are averaged and the average value is used in place of the actual values. This approach maintains layer balance and properly accounts for the effect of design changes on the generalized deflection. In the trial process of finding a value of the target derivative that satisfies Equation (2.8), the layer thickness is not rounded. Rounding is done only after that process is completed, when the layer thickness is rounded up or down to the nearest multiple of the lamina thickness. By rounding both up and down, the effect of rounding on the constrained deflection can be minimized.

The evaluation of the deflection derivatives is carried out in the same way as in ASOP-3, and is explained in Appendix G.3 of Reference 4.

2.3.5.2 Resizing Algorithm for Interacting Deflection, Stress, and Minimum/Maximum Gage Constraints

As stated above, the deflection-constraint mode is entered only if (1) the deflection constraint is an equality constraint ($\delta = \delta_{desired}$), or (2) it is an inequality constraint ($\delta \leq \delta_{desired}$ or $\delta \geq \delta_{desired}$) that is violated by the design existing at the end of the stress-constraint mode. (It should be noted that the subject deflection δ and its desired value $\delta_{desired}$ are algebraic quantities, not absolute values.) It is desirable that the design existing at entry to the deflection-constraint mode should be very nearly a fully stressed design.

If the constraint is an inequality constraint that is violated by the design existing at entry to the deflection-constraint mode, it is treated as an equality constraint in the deflection-constraint mode. It is shown in Appendix G.4 of Reference 4 that this approach should yield a design that is near optimum for the inequality constraint.

Prior to entry into the iterative redesign process, a determination is made of the algebraic sign of the derivatives to be introduced into Equation (2.7), as discussed in Subsection 2.3.5.1. If the current value of the deflection subject to constraint is smaller (algebraically) than the constraint value, positive derivatives are taken. If the current value of the deflection subject to constraint is larger (algebraically) than the constraint value, negative derivatives are taken. Once this determination is made, it remains unchanged throughout the remainder of the procedure, for reasons that will now be discussed.

As long as movement from the initial value of the constrained deflection (upon entry into the deflection-constraint mode) toward the constraint value is in the same direction, it is clear that this sign should not be changed. However, consider the situation where the constraint value is overshot, and movement in the reverse direction becomes necessary? If the sign were to be reversed, all those elements previously resized by the deflection constraint would be suddenly relieved of such constraint, and their gages could drop to values determined by other constraints. Under these circumstances, large changes could be expected to result from a need for minor adjustments, as the amount of overshoot would normally be small. These large changes could

be expected to preclude satisfactory convergence to an optimum design. Maintaining the same sign keeps these adjustments essentially within the same group of elements that have previously been governed by the deflection constraint.

Deflection-constraint resizing and stress-constraint resizing are done sequentially within each cycle in the deflection-constraint mode, with an analysis following each type of resizing. There are thus two analyses performed in each cycle. This cycling is continued until a convergence criterion is satisfied or the number of cycles has reached a specified maximum.

Following stress-constraint resizing, the member gages determined on the basis of the stress constraints are treated as minimum gages in the subsequent resizing for the deflection constraint. Similarly, following deflection-constraint resizing, the member gages determined on the basis of the deflection are treated as minimum gages in the subsequent resizing for stress constraints. Continued to convergence, this process effectively takes into account the interaction between the deflection constraint and stress constraints. It can be seen that, upon entry into the first cycle of the deflection-constraint mode, deflection-constraint resizing cannot reduce any gages, as they are then all governed either by stress constraints or by minimum gage constraints. However, in subsequent cycles, reductions can be made in gages previously governed by the deflection constraint. Such reduction, however, is not permitted to bring a gage below the largest of the following: the gage as determined on the basis of stress constraints, the specified minimum gage, and a "MAX CUT" value.

The "MAX CUT" value is determined by multiplying the gage prior to resizing by a factor that is specified by the user and has a value between 0 and 1. Its intent is to provide the user with a means of limiting the reduction that a single resizing step can effect in any gage, in the event that excessive reductions cause an instability in the iterative solution.

The algorithm applied in the deflection-constraint mode is illustrated in flow-chart form in Figures 2.4 and 2.5 and is explained in detail in Reference 4. Figure 2.4 shows the algorithm for alternating deflection-constraint and stress-constraint resizing, while Figure 2.5 focuses on the deflection-constraint resizing portion of the cycle.

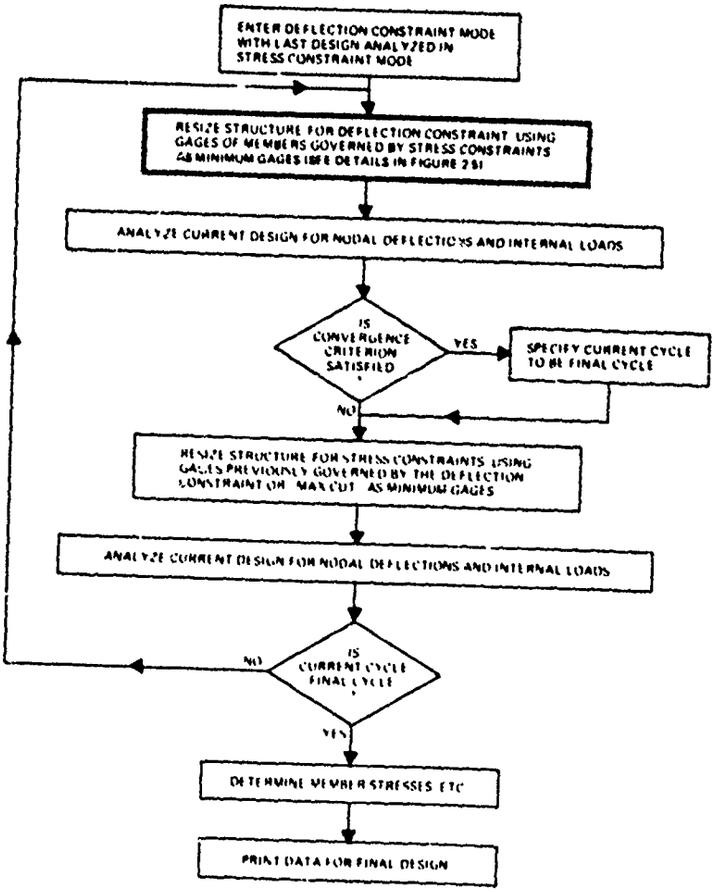

Figure 2.4 Iteration Cycles in Deflection-Constraint Mode (Alternating Deflection-Constraint and Stress-Constraint Resizing)

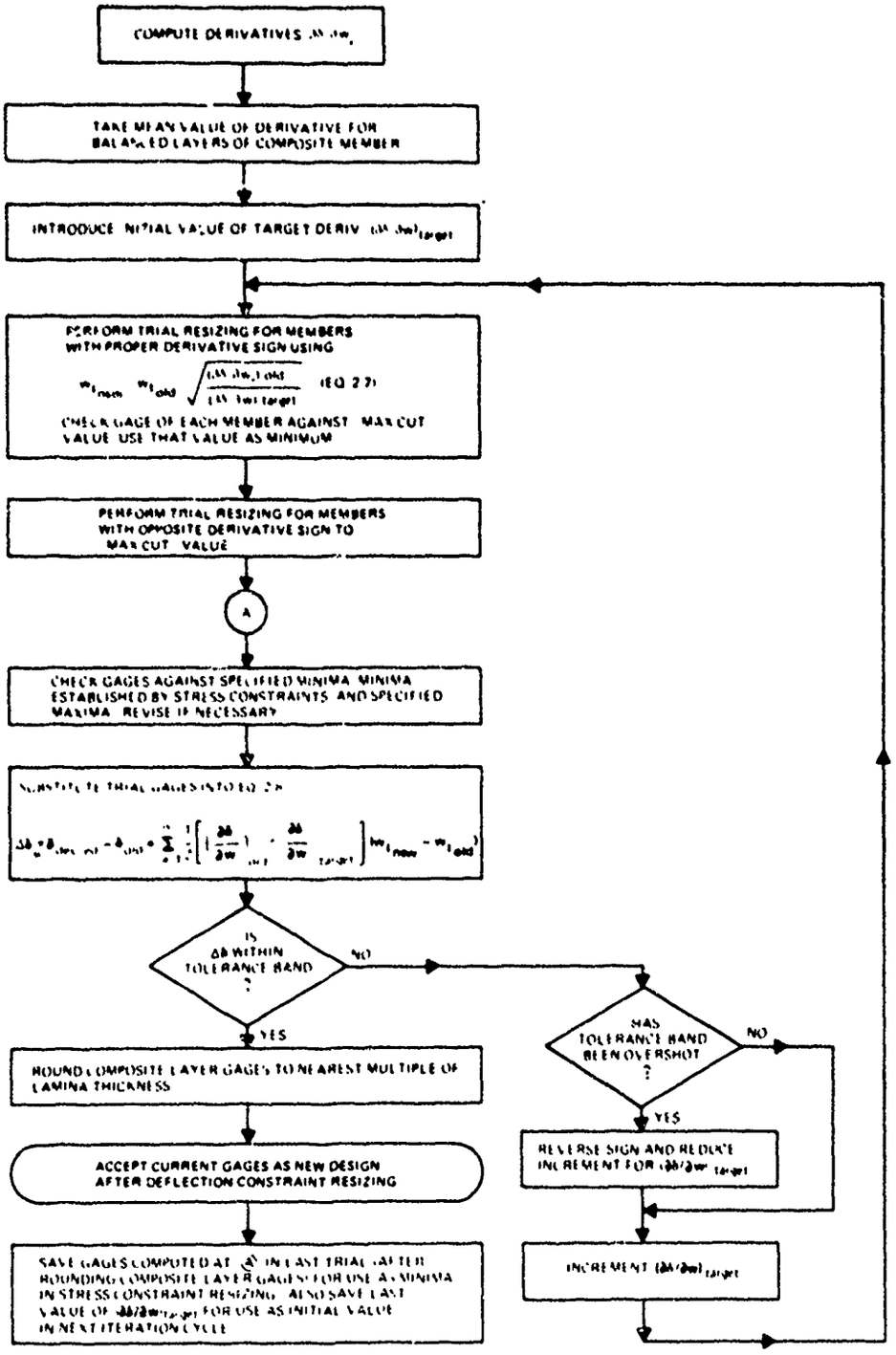

Figure 2.5 Algorithm for Deflection-Constraint Resizing

The alternating application of deflection and stress constraints, with the gages determined by one being used as minimum gages in the other, as described above, converges to a design in which there are two classes of elements (or layers in the case of composites). One class comprises elements that are fully stressed or are at minimum or maximum specified gage. The other class comprises elements that are governed by the deflection constraint. In this latter class, the derivatives of deflection with respect to element (or layer) weight all have nearly uniform values. Departures from uniformity are due to lack of convergence or, in the case of composite element layers, to rounding to an integral number of laminae. Under these circumstances, it can be expected that the design will be close to optimum, at least in a local, if not in a global, sense.

It should be noted that an option in the program permits the designation of selected members as noncandidates for deflection-constraint resizing, although they are still subject to the application of stress constraints in each cycle in the deflection-constraint mode, unless their gages are being explicitly fixed. This option is useful, for example, when designing structures having fixed-gage honeycomb core substructure that is idealized using shear panels. Another useful application is described in the following subsection.

2.3.5.3 Treatment of Multiple Deflection Constraints as a Succession of Single-Constraint Problems

Although only a single deflection constraint, in a single loading condition, can be treated in one submission of the program, as discussed above, it is possible to treat special cases of multiple deflection constraints by making multiple submissions of the program. The special cases are those in which the constraints can be ordered, so that the first constraint can be satisfied, after which a portion of the structure can be frozen in design to prevent further change in the corresponding deflection; then the second constraint can be satisfied by redesign of the remaining structure, after which a portion of that structure can be frozen in design, to prevent further change in the corresponding deflection; and so on, until the last constraint is satisfied. Clearly, cantilever structures, particularly slender ones, with deflection constraints such as angles of twist applied at two or more stations along the span, fit this situation to some degree of approximation.

The program must be submitted for execution as many times as there are constraints to be satisfied. In each submission, the design variables are initialized at the final values they had in the preceding submission, and, in the case of those design variables that are nominally to be frozen, their newly initialized values are also their minimum values. The word "nominally" is used because, while these design variables are removed from candidacy for deflection-constraint resizing, they are not truly frozen, as it is still necessary to apply stress constraints to them if overstress is not to occur. This may have the effect of further altering the deflections already set at their constraint values, but this effect can generally be expected to be small.

The process of making successive submissions has been largely automated in FASTOP-3, unlike ASOP-3 where there is a great deal of data manipulation required in each submission. The design produced by each submission is stored on a permanent data set and used as input data to the next submission. Relatively little additional card data are needed in each subsequent submission.

2.3.6 Flexible Supports

In the resizing of a wing structure connected redundantly to a fuselage, it is important that the interactive forces at the points of connection be properly determined. A similar situation occurs in other cases, such as those of wing or tail surfaces with flexible control surfaces or stores attached in such a manner that the interactive forces are statically indeterminate.

A capability of accommodating this type of situation has been incorporated into FASTOP-3. Nodes that are at points of elastic support or points of connection to adjoining elastic structure are considered to be free to displace, but additional stiffnesses representing the constraints applied by the supports or adjoining structure must be supplied by the user. These additional stiffnesses are inserted at the appropriate locations in the structure stiffness matrix. In the case of statically indeterminate forces of interaction with adjoining structure, there will generally be cross-coupling between the degrees of freedom at the points of connection.

2.4 TRANSFORMATIONS BETWEEN MATHEMATICAL MODELS

Except for some minor changes in the required input data, the transformation procedures in FASTOP-3 are identical to those of FASTOP-1. Four distinct math models are involved in these transformations, namely an aerodynamics model, a weights model (for inertial loads), a structures models, and a dynamics model. Three transformation matrices can be created, which respectively transform loads from the aerodynamics, weights, and dynamics models to the structures model. The first two matrices are needed for the computation of applied loads, whereas the third matrix is used in the computation of a dynamics model flexibility matrix. A comprehensive treatment of the transformation procedures is presented in Section 5 of Reference 1.

2.5 MASS MATRIX DEFINITION

The procedure for obtaining a dynamics-model mass matrix for use in vibration analysis has not changed in FASTOP-3. There are two alternate methods for obtaining this matrix, namely the "standard" approach and the "fully automated" approach. In the standard approach, the user supplies the mass matrix for the "initial" design, i.e., for the design as it exists prior to any automated flutter resizing. In the fully automated approach, this matrix is computed automatically within the program, based on the weights of the structural members (including non-optimum factors, if any), plus any fixed-mass items and mass-balance weights supplied by the user. Regardless of which approach is used, the program automatically updates the initial mass matrix to account for the cumulative weight changes due to all flutter and strength resizing beyond the initial design. See Section 6 of Reference 1 for the details of the procedure.

2.6 VIBRATION ANALYSIS

The vibration analysis procedure described in detail in Section 7 of Reference 1 applies to FASTOP-3 as well. Up to 200 dynamic degrees of freedom can be accommodated. Both cantilever and free-free type analyses can be carried out, each using either the "flexibility" approach or the "stiffness" approach. For the flexibility approach, the user must specify a separate dynamics model, and the eigenvalue problem is then formulated in terms of a

dynamics-model flexibility matrix. The stiffness approach is employed when the user does not choose to provide a separate dynamics model. In that case, the dynamic degrees of freedom are taken to coincide with all the structures-model degrees of freedom, and the eigenvalue problem is formulated in terms of the structures-model stiffness matrix. The 200-degree-of-freedom limitation mentioned earlier obviously restricts the stiffness approach to problems in which simple structures models are used.

2.7 FLUTTER ANALYSIS

Except for the improvements described below, the flutter analysis capabilities of FASTOP-3 are the same as those of FASTOP-1, which are described in Section 8 of Reference 1. The program determines the oscillatory pressures and the generalized aerodynamic forces for the lifting surface to be analyzed, given a set of normal mode shapes and frequencies. Generalized aerodynamic forces are computed using either the subsonic assumed-pressure-function procedure (kernel function), the supersonic Mach-box method or the subsonic doublet-lattice procedure. Then, given the generalized masses corresponding to the modes, the program solves the flutter equation to determine the flutter speed and values of modal damping and frequency as functions of air speed. Flutter solutions are obtained by use of either the conventional k-method or an improved version of the p-k method. In the latter method, which is used for redesign purposes, the eigenvectors and their associated row vectors are determined at the flutter speed for use in computing flutter-velocity derivatives.

2.7.1 Improvements to the p-k Solution Algorithm

In FASTOP-3, improvements have been introduced into the p-k solution algorithm, specifically with respect to root tracking and with respect to rigid-body modes. Modifications have been made to the root tracking logic because it was discovered that the original logic, under some circumstances, could lead to incorrect identification of the critical root. Moreover, with the new logic, the roots are generally determined after fewer iterations, and there is more certainty that roots are properly ordered at all velocities. Modifications have also been made to permit inclusion of zero-frequency rigid-body modes in the p-k flutter calculations.

2.7.2 An Improvement to the Mach-box Aerodynamics Procedure

Studies using the Mach-box routines in FASTOP-1 showed that erratic undulations occurred frequently in the computed pressure distributions. Accordingly, for FASTOP-3, these routines were modified so as to greatly improve the pressure distributions while retaining the essential flow discontinuities. As a result of these modifications, some of the text, equations and figures in Subsection 8.2.2 ("Supersonic Mach-Box Program") of Reference 1 are no longer applicable. Accordingly, a revised version of that entire subsection is presented on the following pages.

2.7.2.1 Revised Supersonic Mach-box Program for FASTOP-3

For the supersonic regime, the aerodynamics program used is a modified version of the Mach-box procedure described in Reference 10. For a harmonically oscillating planar surface, the pressure is related to the velocity potential, and thence to the downwash distribution, by

$$p(x, y) = 2\rho \left(U \frac{\partial}{\partial x} + i\omega\right) \varphi(x, y)$$

$$= \frac{-2\rho}{\pi} \left(U \frac{\partial}{\partial x} + i\omega\right) \iint_S \bar{w}(\xi, \eta) \cdot e^{\frac{-i\omega M^2}{U\beta^2}(x-\xi)} \cdot \frac{\cos \frac{\omega M}{U\beta^2} R}{R} \, d\xi \, d\eta$$

$$\text{or} \quad C_p(x,y) = \frac{-4}{\pi} \left(\frac{\partial}{\partial x} + i \frac{\omega}{U}\right) \iint_S w(\xi, \eta) \cdot e^{-i \frac{\omega M^2}{U\beta^2}(x-\xi)} \cdot \frac{\cos \frac{\omega M}{U\beta^2} R}{R} \, d\xi \, d\eta, \tag{2.9}$$

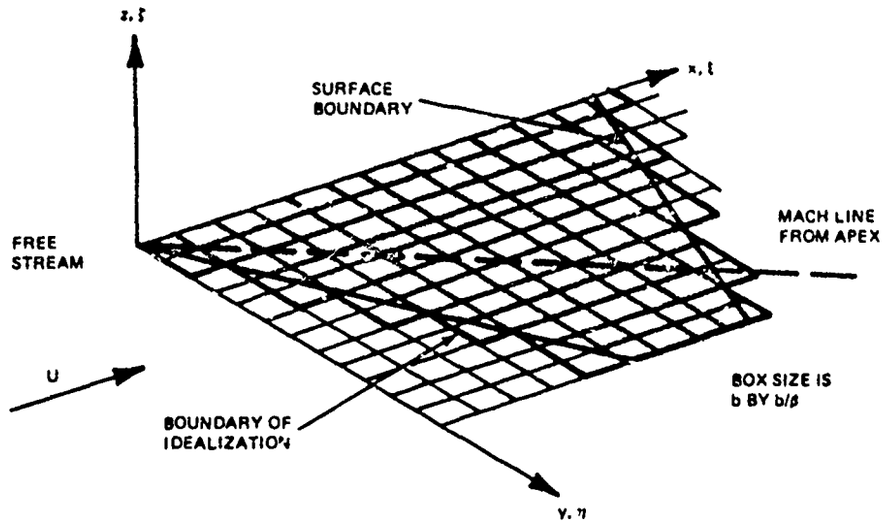

Figure 2.6 Mach-Box Grid for a Lifting Surface

where

x, ξ are streamwise coordinates

y, η are spanwise coordinates

p is the differential pressure between the upper and lower covers of the surface

ρ is the air density

U is the free-stream velocity

ω is the frequency of oscillation

ϕ is the velocity potential

S is the lifting-surface area bounded by the inverse Mach cone emanating from (x, y)

$\tilde{w}$ is the complex downwash velocity = $U\alpha + i\omega h = Uw$

h, α are the deformation and slope of the surface

M is the Mach number

$\beta = \sqrt{M^2-1}$

$R = \sqrt{(x-\xi)^2 - \beta^2 (y-\eta)^2}$.

C_p is the differential pressure coefficient = $p/(1/2\rho U^2)$

With the exception of special cases, the integral cannot be evaluated in closed form; hence, a numerical approach is required. In Reference 10, the area, S, is divided into elementary small rectangular boxes having their diagonals parallel to the Mach lines as shown in Figure 2.6. The rectangles are subsequently converted to squares through the coordinate transformations

<u>Streamwise</u> $\tilde{x} = x/b$,

$\tilde{\xi} = \xi/b$,

<u>Spanwise</u> $\tilde{y} = \beta y/b$

$\tilde{\eta} = \beta\eta/b$, (2.10)

where b is the streamwise dimension of a box and b/β is the spanwise dimension.

Assuming the downwash is constant over each of these "Mach boxes," Equation (2.9) can be rewritten as:

$$C_p(\tilde{x}, \tilde{y}) = \frac{-4}{\pi}\sum_j w_j \left[\frac{1}{b}\frac{\partial}{\partial \tilde{x}} + i\frac{\omega}{U}\right] \cdot \iint_{S_j} e^{-i\tilde{k}(\tilde{x}-\tilde{\xi})} \cdot \frac{\cos\frac{\tilde{k}\tilde{R}}{M}}{\tilde{R}\cdot b} \cdot \frac{b^2}{\beta}\, d\tilde{\xi}\, d\tilde{\eta},$$

$$C_p(\tilde{x}, \tilde{y}) = \frac{-4}{\beta\pi}\sum_j w_j \left(\frac{\partial}{\partial \tilde{x}} + ik\right) \iint_{S_j} e^{-i\tilde{k}(\tilde{x}-\tilde{\xi})} \cdot \cos\frac{\tilde{k}\tilde{R}}{M} \cdot \frac{d\tilde{\xi}\, d\tilde{\eta}}{\tilde{R}}, \tag{2.11}$$

or $$C_p(\tilde{x}, \tilde{y}) = \sum_j w_j C_j(\tilde{x}, \tilde{y}), \tag{2.12}$$

where

S_j is the j^{th} box within the inverse Mach cone emanating from $(\tilde{x}, \tilde{y})$

$k = \frac{\beta\omega}{U}$

$\tilde{k} = \left(\frac{M}{\beta}\right)^2 k$

$\tilde{R} = \sqrt{(\tilde{x}-\tilde{\xi})^2 - (\tilde{y}-\tilde{\eta})^2}$

b is the streamwise box size

w_j is the downwash on the j^{th} box

C_j is the j^{th} pressure influence coefficient for point $(\tilde{x}, \tilde{y})$, i.e., the pressure at the point due to a unit downwash on the j^{th} box.

Two methods have been classically used to perform the complex integration over the box area. The first, developed in Reference 11, uses a mean value of the exponential and cosine terms when a box is far removed from the point $(\tilde{x}, \tilde{y})$ and a series expansion up to k^2 when a box is close. Although these approximations simplify the integration, they introduce significant errors when the reduced frequency, k, is high. For a more exact evaluation, a second method, a Bessel-function series representation of the integral, is presented in Reference 10.

The method used in the current program is different from both of these two in that Gaussian quadrature is used to evaluate the integral. With this technique, singularities that occur in the integrand when the box area is cut or touched by the inverse Mach cone emanating from the point $(\tilde{x}, \tilde{y})$ - see Figure 2.7a - can be accurately accounted for as described below. In fact, if the integrand could be represented exactly by the product of a simple singular function, such as $1/\sqrt{1-y}$, and a polynomial of order 2N-1, then using N integration points would produce the integral with no error. Although the true integrand cannot be presented exactly in the above manner, by taking enough integration points the error may be made as small as desired.

First, the pressure influence coefficient of Equation (2.11) is rewritten by performing a change of variables:

$$C_j(\tilde{x},\tilde{y}) = -\frac{4}{\beta\pi}\left(\frac{\partial}{\partial\Delta x} + ik\right)\int_{m-\frac{1}{2}}^{m+\frac{1}{2}}\int_{\ell-\frac{1}{2}}^{\ell+\frac{1}{2}} e^{-ik\tilde{\Delta}x}\cdot\cos\frac{\tilde{k}\tilde{R}}{M}\cdot\frac{d\Delta x}{\tilde{R}}\,d\Delta y,$$

$$= -\frac{4}{\beta\pi}\,ik\int_{m-\frac{1}{2}}^{m+\frac{1}{2}}\int_{\ell-\frac{1}{2}}^{\ell+\frac{1}{2}} e^{-ik\tilde{\Delta}x}\cdot\cos\frac{\tilde{k}\tilde{R}}{M}\cdot\frac{d\Delta x\,d\Delta y}{\tilde{R}}$$

$$-\frac{4}{3\pi}\,e^{-ik(\ell+\frac{1}{2})}\int_{m-\frac{1}{2}}^{m+\frac{1}{2}}\cos\frac{\tilde{k}\tilde{R}_{\ell+\frac{1}{2}}}{M}\cdot\frac{d\Delta y}{\tilde{R}_{\ell+\frac{1}{2}}}$$

$$+\frac{4}{\beta\pi}\,e^{-ik(\ell-\frac{1}{2})}\int_{m-\frac{1}{2}}^{m+\frac{1}{2}}\cos\frac{\tilde{k}\tilde{R}_{\ell-\frac{1}{2}}}{M}\cdot\frac{d\Delta y}{\tilde{R}_{\ell-\frac{1}{2}}},$$

(2.13)

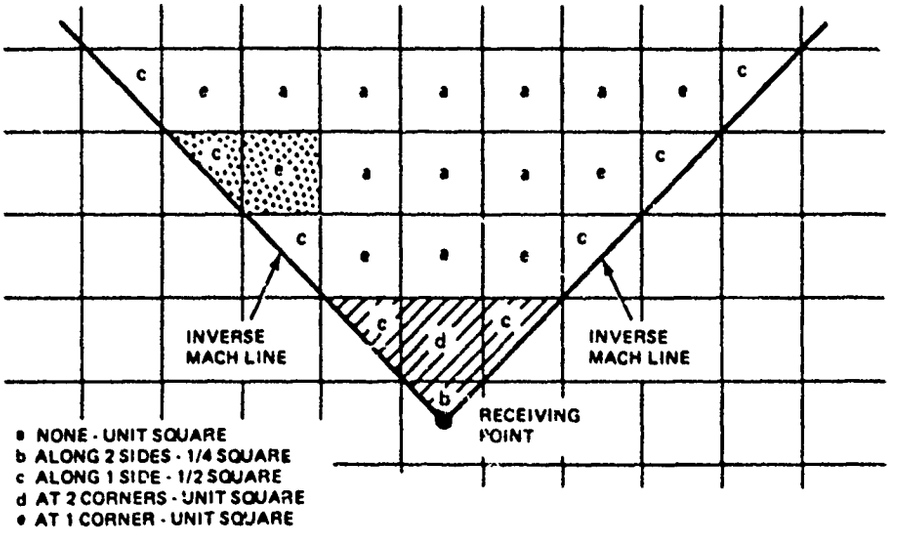

(a) Type of Singularity and Integration Area

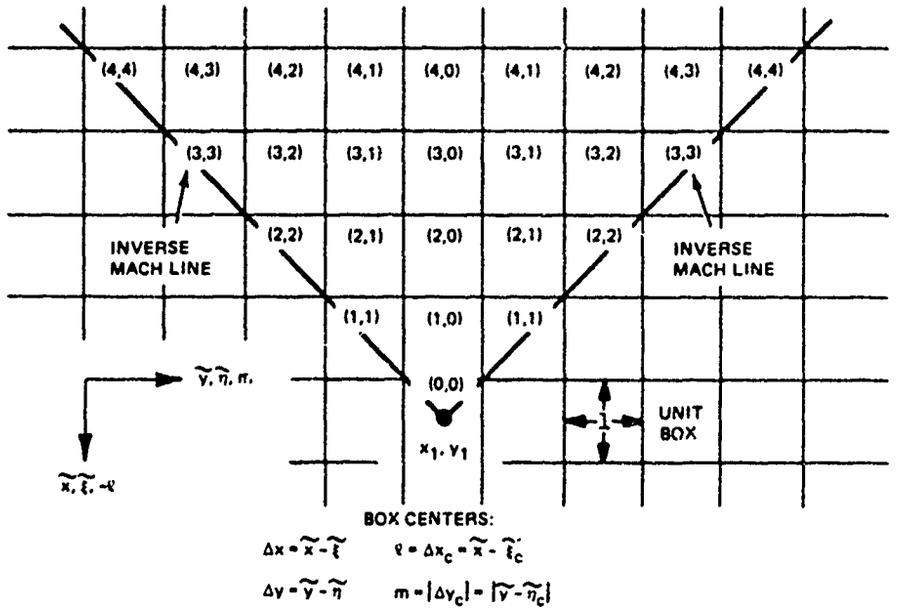

(b) Local Mach-Box Coordinates for Arbitrary Receiving Point

Figure 2.7 Singularities and Coordinate System for Mach-Box Formulation

where

$$\Delta x = \tilde{x} - \xi$$

$$\Delta y = \tilde{y} - \eta$$

ℓ, m are the components of the distance between the j^{th} box center and the point $(\tilde{x}, \tilde{y})$ - see Figure 2.7b.

$$\tilde{R}_{\ell} = \sqrt{(\ell + \tfrac{1}{2})^2 - (\tilde{y} - \tilde{\eta})^2}$$

$$\tilde{R}_{-\ell} = \sqrt{(\ell - \tfrac{1}{2})^2 - (\tilde{y} - \tilde{\eta})^2}$$

Next, the two single and one double integrations are performed using various quadrature formulae of Reference 12. Referring to Figure 2.7a, five cases can arise depending on how the sending box is cut by the inverse Mach cone from $(\tilde{x}, \tilde{y})$:

(a) Box not touched: $\ell \geq 2$, $m \leq \ell - 2$.

(b) Box at apex of the cone: $\ell = 0$, $m = 0$.

(c) Box split by the cone: $\ell = m$, $m > 0$.

(d) Box touched at two corners by the cone: $\ell = 1$, $m = 0$.

(e) Box touched at one corner by the cone: $\ell > 1$, $m = \ell - 1$.

In case (a), since there is no singularity, the following quadrature formula (Equation 25.4.30, Reference 12) may be used for both the spanwise and chordwise integrations:

$$\int_a^b f(y)\, dy = \frac{b-a}{2} \sum_{i=1}^{n} H_i \cdot f(y_i), \qquad (2.14)$$

where

$$y_i = \frac{b-a}{2} x_i + \frac{b+a}{2}$$

x_i is the i^{th} zero of the Legendre polynomial, P_n

H_i, the weighting function at the i^{th} quadrature point,

$$= 2/(1 - x_i^2) \left[P_n' (x_i) \right]^2$$

In case (b), the integration is to be performed only on the triangular area of a quarter-box. Hence, reversing the order of integration in Equation (2.13), the limits of the double integral become $\int_0^{\frac{1}{2}} \int_{-\Delta x}^{\Delta x}$, while the limits of the single integral are $\int_{-\frac{1}{2}}^{\frac{1}{2}}$. Since R = 0 at the limits Δx and $-\Delta x$, and since $R_{1/2} = R_{-1/2} = 0$ at the limits 1/2 and -1/2, the spanwise integrals have singularities, and a different quadrature formula (Equation 25.4.39, Reference 12) is used:

$$\int_a^b \frac{f(y)\,dy}{\sqrt{(y-a)\,(b-y)}} = \sum_{i=1}^{n} H_i \; f(y_i), \qquad (2.15)$$

where

$$y_i = \frac{b-a}{2}\, x_i + \frac{b+a}{2}$$

$$x_i = \cos\,(2i-1)\,\frac{\pi}{2n}$$

$$H_i = \pi/n.$$

After the spanwise integration is performed, Formula (2.14) is used in the chordwise direction.

For case (c), the integration is done over a triangular half-box where the limits of the integrals become $\int_{\ell-\frac{1}{2}}^{\ell+\frac{1}{2}} \int_{\ell-\frac{1}{2}}^{\Delta x}$ and $\int_{\ell-\frac{1}{2}}^{\ell+\frac{1}{2}}$. Since the spanwise integrals here have singularities at the upper limits only, the appropriate quadrature formula (Equation 25.4.37, Reference 12) is:

$$\int_a^b \frac{f(y)\,dy}{\sqrt{b-y}} = \sqrt{b-a} \sum_{i=1}^{n} 2\, H_i^{(2n)} \; f(y_i), \qquad (2.16)$$

where

$y_i = a + (b-a)(1-x_i^2)$

x_i is the i^{th} positive zero of the Legendre polynomial, P_{2n}.

$H_i^{(2n)}$ are the Gaussian weights of order 2n.

Again, Formula (2.14) is used in the chordwise integration.

For case (d), an integration is first performed over the triangular shaded area in Figure 2.7a (comprising boxes b, c, and d) using the quadrature formulae for case (b). Then by subtracting the previously derived pressure influence coefficients for boxes b and c, the desired integral over d is achieved.

Finally, for case (e), the integral for an aggregate area (see dotted area in Figure 2.7a) consisting of a triangle on the Mach line and the subject area is determined; and from it the integral for a triangle is subtracted. When the spanwise integrations are performed, Equation (2.16) is employed, while Equation (2.14) is used in the chordwise direction.

For case (a) and all chordwise integrations, the present program uses six integration points for the quadrature. In the spanwise integrations, six points are used when $k < \frac{4}{3}(\frac{\beta}{M})^2$, while twelve points are employed when $k \geq \frac{4}{3}(\frac{\beta}{M})^2$.

At a given Mach number and reduced frequency, the pressure influence coefficients are functions of only ℓ and m - the separation between the sending and receiving box centers. Consequently, influence coefficients are computed by the above formulae only once for each admissible ℓ, m pair ($\ell \geq 0$, $m \leq \ell$) and are used repeatedly where needed.

The pressure on any box is a function of the downwash of only those boxes within the inverse Mach cone emanating from its box center. For a surface, the edges of which are all supersonic, the pressure is, furthermore, only influenced by boxes on the planform. If any of the surface edges are subsonic, however, there are regions adjacent to these edges which do affect the pressure of some areas on the planform. To account for this effect, the concept (Reference 13) of a permeable "diaphragm" is introduced in these regions. This permeable sheet does not alter the flow nor can it sustain

pressure. It is bounded by the surface edge and the Mach lines emanating from the corners of the lifting surface - see Figure 2.8.

The relationship between the pressure and downwash on the combination of the lifting surface and the diaphragm area can be written:

$$\begin{Bmatrix} P_W \\ \hline P_D \end{Bmatrix} = \begin{bmatrix} C_{WW} & C_{WD} \\ \hline C_{DW} & C_{DD} \end{bmatrix} \begin{Bmatrix} w_W \\ \hline w_D \end{Bmatrix} \qquad (2.17)$$

where

P_W is the pressure on the wing boxes

P_D is the pressure on diaphragm boxes

C_{WW} are the influence coefficients giving pressures on the wing boxes due to downwash on the wing boxes

C_{WD} are the influence coefficients giving pressures on the wing boxes due to the downwash on the diaphragm boxes

C_{DW} are the influence coefficients giving pressures on the diaphragm boxes due to downwash on the wing boxes

C_{DD} are influence coefficients giving pressures on the diaphragm boxes due to downwash on the diaphragm boxes

w_W is the known downwash on the wing boxes

w_D is the unknown downwash on the diaphragm boxes.

Since the pressure on any diaphragm box is zero, then

$$\left[C_{DW}\right] \left\{w_W\right\} + \left[C_{DD}\right] \left\{w_D\right\} = \left\{0\right\}, \qquad (2.18)$$

and the unknown diaphragm downwash can be evaluated by

$$\left\{w_D\right\} = - \left[C_{DD}\right]^{-1} \left[C_{DW}\right] \left\{w_W\right\} \qquad (2.19)$$

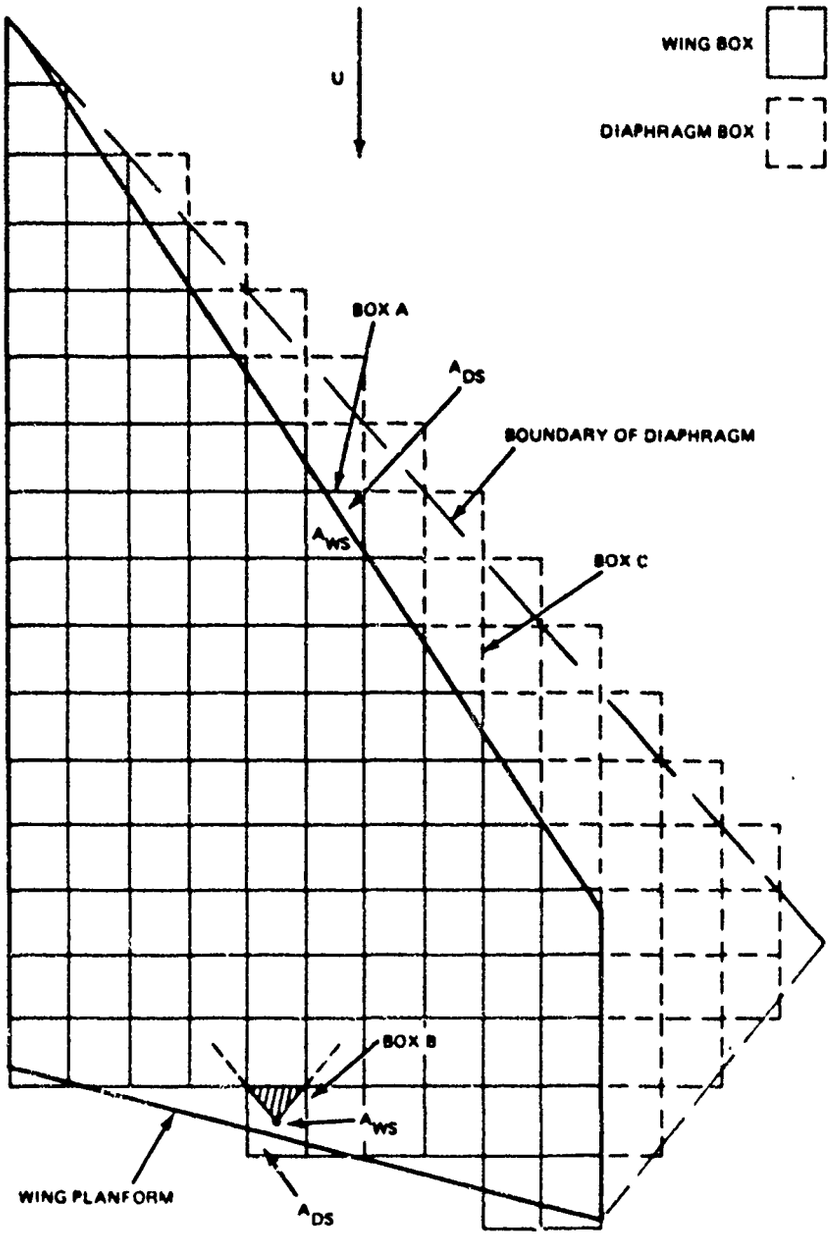

Figure 2.8 Box Allocation for Subsonic Leading Edge

Substituting this result into Equation (2.17) yields the final expression for the pressures on the wing boxes:

$$\{P_W\} = [AIC]\{w_W\} \tag{2.20}$$

where

$$[AIC] = [C_{WW}] - [C_{WD}][C_{DD}]^{-1}[C_{DW}] \tag{2.21}$$

For maximum computer efficiency, the actual calculation of the pressures, P_W, is generally performed in a different manner from that implied by Equation (2.20). The calculation of the aerodynamic influence coefficient matrix, [AIC], leads to either extensive use of core in storing matrices or a large number of I/O operations if the matrices are stored on data devices. If there is no need for saving the [AIC] array for future use, the machine operations can be appreciably reduced by computing the pressures as follows:

$$\begin{aligned}
&(1) \quad \{X\} = [C_{DW}]\{w_W\} \\
&(2) \quad \{Y\} = [C_{DD}]^{-1}\{X\} \\
&(3) \quad \{Z\} = [C_{WD}]\{Y\} \\
&(4) \quad \{P_W\} = [C_{WW}]\{w_W\} - \{Z\}
\end{aligned} \tag{2.22}$$

In this way, core storage requirements are minimized, since only a vector need be stored in going from one step to another.

Once the oscillatory pressures are computed, the normalized generalized aerodynamic forces are computed by

$$\bar{Q}_{rs} = \frac{-b^2}{2k^2} \iint_{S/2} h_r(x, y)\, C_{p_s}(x, y)\, dx\, dy. \tag{2.23}$$

Since the boxes are assumed to be very small, the integration can be replaced by a summation over every box on the planform:

$$\bar{Q}_{rs} = -\frac{b^2}{2k^2} \sum_{j} h_r^{(j)} \, w_s^{(j)} \, A^{(j)}, \tag{2.24}$$

where

$h_r^{(j)}$ is the deflection of the j^{th} box in the r^{th} mode

$C_{p_s}^{(j)}$ is the pressure coefficient of the j^{th} box in the s^{th} mode

$A^{(j)}$ is the area of the j^{th} surface box.

It should be noted that each box area is b^2/β. The program automatically establishes the gridwork of boxes: From a user specified number of boxes desired, the program calculates the box size necessary for the boxes to cover the planform and diaphragm and to align with the inboard and outboard planform edges. Consequently, no boxes overhang the planform side-edges. (See Figure 2.8.) Each box is designated as either a wing box or diaphragm box depending on whether its center lies on or off the wing, respectively. In general, boxes do overhang the leading and trailing planform edges causing, in effect, a jagged representation of these edges. Although for most configurations, this jaggedness has been found to have little effect on the accuracy of the generalized aerodynamic forces for simple mode shapes, providing that the box grid is not too coarse, it does produce erratic undulations in the computed pressures.

A recent analytical refinement (see Reference 14) remedies this shortcoming of the basic method, and produces greatly improved supersonic oscillatory pressure distributions with only a nonimal increase in computer time. This refinement, which has been incorporated into FASTOP-3, is described as follows:

Any box that is crossed by a planform edge is considered to consist of two identical overlapping boxes, one being treated as if it were on the planform and the other as if it were on the diaphragm. Let the pressures, downwashes, and influence coefficients for such boxes be denoted by the subscripts WS (wing, shared) and DS (diaphragm, shared). Now, since the area of the planform encaptured by a box, WS_i, is only a fraction, A_{WS_i}/A, of the full box area (see box A, Figure 2.8), the contribution to the pressure at any other box due to a signal originating from this box should be scaled by this ratio. Although similar reasoning might be applied to the box DS_i, it has been demonstrated in sample calculations that this scaling should only be applied to the wing-shared boxes. Incorporating these ideas, Equation (2.17) is replaced by

$$\begin{Bmatrix} P_W \\ \hline P_{WS} \\ \hline P_{DS} \\ \hline P_D \end{Bmatrix} = \left[\begin{array}{c|c|c|c|c} [C_{WW}] & [C_{WWS}] \cdot [A_{WS}] & 0 & [C_{WD}] \\ \hline [C_{WSW}] & [C_{WSWS}] \cdot [A_{WS}] & 0 & [C_{WSD}] \\ \hline [C_{DSW}] & 0 & [C_{DSDS}] & [C_{DSD}] \\ \hline [C_{DW}] & 0 & [C_{DDS}] & [C_{DD}] \end{array}\right] \begin{Bmatrix} w_W \\ \hline w_{WS} \\ \hline w_{DS} \\ \hline w_D \end{Bmatrix} \quad (2.25)$$

where the factors of 1/A are omitted since the area of a full box in the transformed Mach-box system is identically unity. The zero submatrices in this equation are necessary to assure non-zero leading-edge pressures. For further explanation, refer to Reference 14.

An additional distinction in handling boxes is required to properly treat trailing edges. For a typical box on a supersonic trailing edge, the inverse Mach cone from a point at the center of the box encompasses the same wing area, A/4, as does any upstream whole wing box (see shaded area in box B, Figure 2.8). Since the downwash on such a box affects the pressure on almost no other box, the area ratio is not applied to the influence coefficient of this box. For a box on a subsonic trailing edge, the wing area encompassed by the inverse Mach cone is still generally a much larger percentage of the total Mach cone area than is indicated by the ratio, A_{WS}; hence, the influence coefficient for this box is also not scaled.

Results obtained by the above formulation require some interpretation. Because of the jagged representation of the leading edge, the centers of some boxes, such as box C, Figure 2.8, lie physically ahead of the true planform; yet, non-zero pressures are computed for such boxes. This is correct, since the calculated pressure coefficient, P_{WS}, is applied over the entire box area and, certainly, the pressure over A_{WS} is non-zero. Now, if the force $P_{WS} \cdot A$ is applied to only the correct area, A_{WS}, the true pressure coefficient for that area would be $P_{WS} \cdot A/A_{WS}$, or, since $A = 1$, P_{WS}/A_{WS}. However, since the contribution from such shared boxes to the generalized force is given by

$$\begin{aligned} Q &= \left([A_{WS}] \cdot \{P_{WS}/A_{WS}\} \right)^T \cdot \{h_{WS}\} \\ &= \{P_{WS}\}^T \cdot \{h_{WS}\}. \end{aligned} \quad (2.26)$$

the pressures computed by solving Equation (2.25) rather than the weighted values, P_{WS}/A_{WS}, are actually used in the computer program.

Results of numerous examples in Reference 14 show that the pressure distributions obtained from the present method are substantially better than those computed by the basic method.

When a highly swept surface is analyzed for a relatively low Mach number, the number of forward diaphragm boxes can become so great as to cause an appreciable increase in computing time. However, the downwash in the diaphragm region decreases very rapidly in the forward streamwise direction. To save computing time, the present program takes this rapid decay of diaphragm downwash into account and allows the user to request a box-elimination option whereby the diaphragm boxes are ignored forward of a user-specified distance ahead of the leading edge.

In the program, provision is made for computing aerodynamic force coefficients and center-of-pressure locations. The user may use this facility to compare known steady-state data with computed values to determine the number of boxes required for a satisfactory solution. Another approach is to vary the number of boxes and look for convergence in the stability coefficients.

2.8 RESIZING FOR COMBINED FLUTTER AND STRENGTH REQUIREMENTS

Except for a few details regarding the treatment of composite members the procedure described in Section 9 of Reference 1 for effecting interactive strength/flutter redesign still applies in FASTOP-3. However, as this procedure is a major feature of the FASTOP system, it is set forth again below. The reader should consult the original reference for the details of the required computational operations, e.g., computation of flutter-velocity derivatives.

2.8.1 Interactive Strength/Flutter Resizing Procedure

Starting with the use of the Structural Optimization Program (SOP), the structure is sized to satisfy its strength requirements with a fully stressed design. Two categories of elements exist after this first step; specifically, each element either is fully stressed (i.e., "strength-critical") or is at its prespecified minimum gage (as dictated, for example, by manufacturing considerations). The next step uses the Flutter Optimization Program (FOP) to resize structural elements and/or mass-balance design variables to increase the surface's critical flutter speed. None of the structual elements are permitted to be reduced in size in this initial FOP step since, upon entering the step, all of these elements were already either strength-critical* or at prespecified minimum gage. Those structural elements that are increased in size in this step, plus any mass-balance variables present in the design, constitute a third category of elements, namely, "flutter-critical" elements, i.e., elements whose gages are dictated by flutter-speed requirements.

The resizing of some structural elements during the first FOP step may cause a significant redistribution of internal loads within the structure, thereby modifying gage requirements for strength considerations. Accordingly, in the next step, SOP is re-entered for the purpose of a "strength update". This is the first attempt to achieve a minimum weight design that accounts for strength/flutter interaction. In this second SOP step, the flutter-critical elements (and, of course, the minimum-gage elements) are not permitted to be

*In FASTOP-1, member stress ratios were passed from SOP to FOP where they served to define minimum size requirements for strength. In FASTOP-3, these minimums are passed directly, i.e., stress ratios are no longer used in FOP.

resized downward, but the strength-critical elements are free to be sized upward or downward. After resizing, the various elements are reclassified into strength-critical, flutter-critical, and minimum-gage categories. Elements may, of course, change categories. For example, an element would shift from the flutter-critical to the strength-critical set if it had been resized upward to satisfy the modified strength requirements. Likewise, an element which was previously strength-critical might be resized downward to the point where it enters the minimum-gage category.

At this stage, FOP is entered for the second time and the interactive strength/flutter redesign process continues. As in the first FOP step, elements in the strength-critical and minimum-gage categories cannot be sized downward. On the other hand, there now exists a set of elements, namely the flutter-critical elements, which are free to be resized in either direction; if such an element is sized downward, however, its gage is not permitted to fall below the values required by the last strength analysis or by minimum-gage considerations. After resizing, the elements again are reclassified into the three basic categories.

Subsequent interactive application of the two programs proceeds in a manner similar to the second SOP and FOP steps until the process is sufficiently converged. The final design will consist of a set of flutter-critical elements which have nearly uniform flutter-velocity derivatives, a set of strength-critical elements which are fully stressed, and a set of elements which are at prespecified minimum gages.

2.8.2 Flutter Resizing of Composite Members

Flutter resizing of composite members involves a few considerations that have no counterparts for metallic members, namely the "rounding" and "balancing" requirements. These considerations are discussed below.

2.8.2.1 Rounding Requirement

For a composite member, the design variables are the number of laminae in each of the layers. When the flutter resizing equation is applied to such a variable, the new value of the variable will generally not be an integral number of laminae. Accordingly, in FASTOP-3, it has been decided to round the new value to the nearest integer.

2.8.2.2 Balanced-Design Requirement

In the conventional use of FASTOP-3 for strength/flutter redesign, either balanced-laminate resizing or unbalanced-laminate resizing is used consistently throughout the entire redesign process, i.e., for both strength and flutter resizing. The user specifies, by means of clue data in the first SOP pass, which of the two possible types of resizing is to be performed for all subsequent strength and flutter redesign. There is a situation, however, in which departure from this consistent resizing approach may be desirable. Consider the case in which a balanced-laminate fully stressed design has been generated in an initial SOP pass. If this fully stressed design is subsequently found to have a marginal flutter-speed deficiency, the user might wish to resolve the deficiency by merely adding a "patch" of unbalanced material to the design. Accordingly, FOP contains a data clue to make this possible. If that clue is exercised, however, the user logically should not expect to call for further strength resizing in any subsequent pass through SOP, since that program would again generate a balanced design; that is, SOP should thereafter be used to analyze designs only.

When called for, balanced-laminate flutter resizing is accomplished by (a) computing the true flutter-velocity derivatives for the layers to be balanced, (b) averaging these derivatives, and (c) using the average-derivative value when applying the resizing equation to each of the pertinent layers. This procedure is also used for balanced-laminate deflection resizing in SOP.

2.9 USE OF FASTOP FOR INTEGRATED ANALYSIS AND DESIGN

Considerations on the use of FASTOP for interactive strength/flutter redesign, as described in Section 10 of Reference 1, also apply to FASTOP-3. The user-oriented material presented in that reference is intended to guide the user through the entire strength/flutter redesign process. To aid the user, numerous suggestions are provided based on experience obtained during the performance of the demonstration problems.

Section 3

EXAMPLES OF PROGRAM APPLICATIONS

3.1 INTRODUCTION

FASTOP-3 has been applied to two different structures to demonstrate the program's capability to obtain near-optimum designs for metallic and composite lifting surfaces subjected to both strength and flutter-speed requirements. The two cases selected, namely the Intermediate-Complexity Wing and the All-Movable Stabilizer, represent levels of structural detail that would exist at different stages of the design process. Specifically, the coarse model of the wing is representative of the preliminary design phase, whereas the more detailed stabilizer model is typical of what might be used during the later stages of design. The two models and the results of the interactive strength/flutter redesign studies are described in the following subsections. In addition, results are presented for resizing of the Intermediate-Complexity Wing to satisfy deflection constraints.

3.2 INTERMEDIATE-COMPLEXITY WING

3.2.1 Mathematical Models

Figure 3.1 shows the aerodynamic planform and primary structural arrangement of the Intermediate-Complexity Wing. The structures model consists of a cantilevered, symmetric, two-cell box beam, having aluminum substructure and graphite/epoxy composite cover skins in a 0°/±45°/90° layup. The zero-degree fibers are aligned with the center spar of the box. Membrane elements are used to model the skins; shear panels represent the rib and spar webs; and bar elements are introduced between upper- and lower-cover node points. The model has 234 degrees of freedom and 158 members, 64 of which are composite members requiring 4 design variables each.

The dynamics model of the Intermediate-Complexity Wing is shown in Figure 3.2. There are 39 dynamics nodes, each of which lies in the wing mid-plane directly between upper and lower cover structural node points. Every dynamics node is permitted to undergo out-of-plane displacement. In addition, nodes along the perimeter of the wing also have rotational degrees of freedom about either the front spar, rear spar, tip rib, or pitch-axis

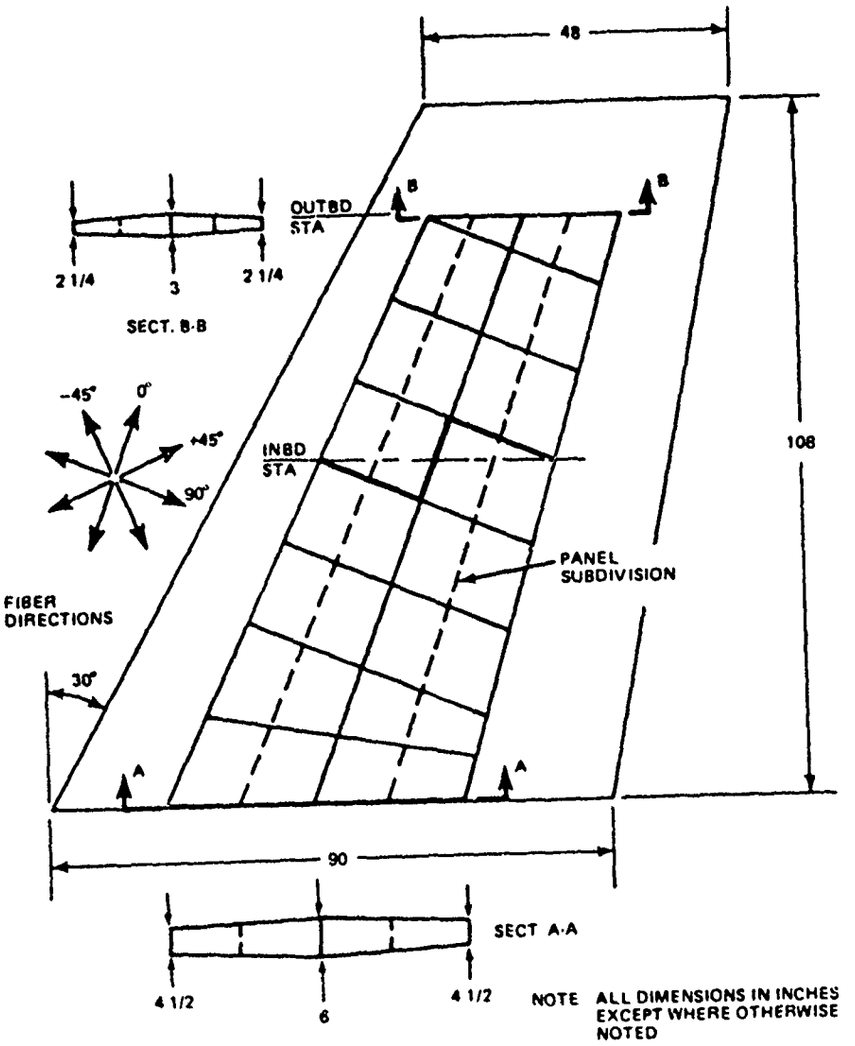

Figure 3.1 Aerodynamic Planform and Primary Structural Arrangement of Intermediate-Complexity Wing

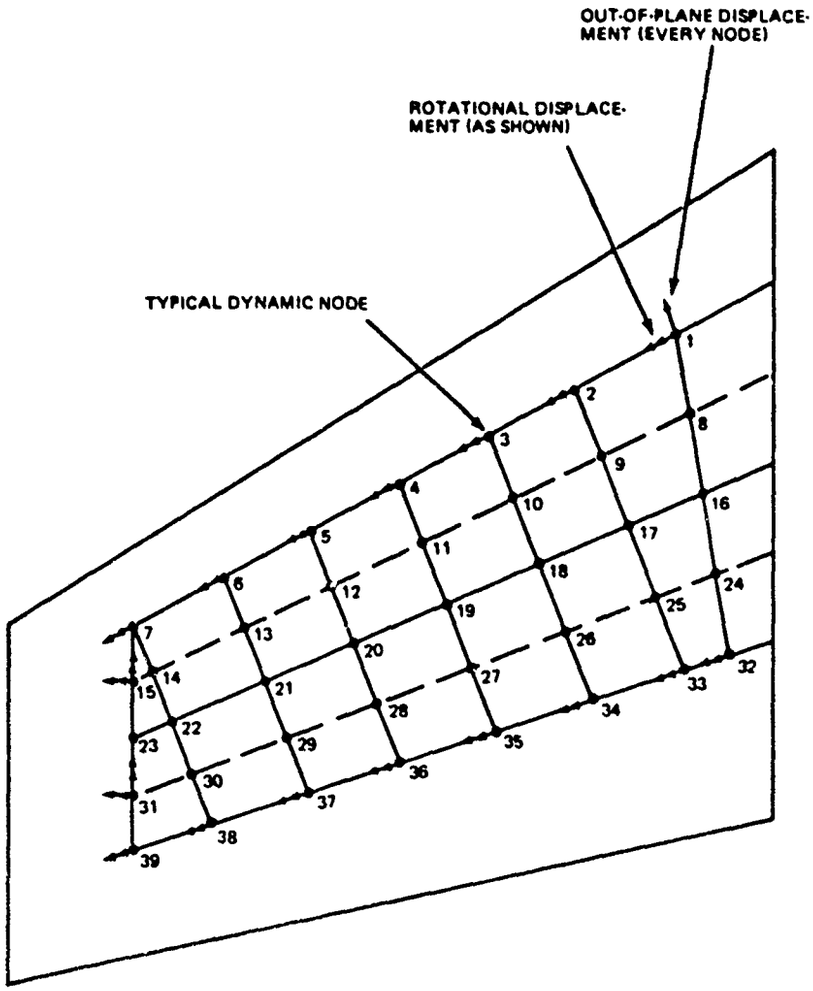

Figure 3.2 Dynamics Model of Intermediate-Complexity Wing

directions. These rotational freedoms are needed to properly account for the mass and inertia of the overhung structure. In all, the dynamics model has 58 degrees of freedom.

3.2.2 Results of Strength/Flutter Redesign Study

Using two applied load conditions (one subsonic and one supersonic) the Structural Optimization Program (SOP) was employed to obtain fully stressed designs (5 FSD cycles) for both the unbalanced- and balanced-laminate options; balancing was with respect to the ±45° layers. The resulting unbalanced design weighed 37.7 lb, 14.3 lb of which went into each of the two identical covers. For the balanced design, the weight was 41.6 lb, each cover weighing 16.3 lb.

The Flutter Optimization Program (FOP) was then used to perform vibration and flutter analyses for both the unbalanced and balanced fully stressed designs. The flutter analyses utilized the doublet-lattice procedure for Mach 0.8, sea level, with the six lowest-frequency normal modes of vibration. For the unbalanced design, the flutter speed was 712 KEAS; the balanced design had a flutter speed of 780 KEAS.

Two parallel interactive strength/flutter redesign studies were then initiated to raise the flutter speeds of both designs to 925 KEAS (1.3 x 712). Flutter resizing was restricted to the composite cover skins only, but all elements were candidates for strength resizing. Figure 3.2 shows a history of the resizing steps for both balanced and unbalanced laminates. In each case, an efficient final design was obtained in 6 combined strength/flutter resizing steps. The first 3 steps in each study were used to raise the flutter speed from the FSD value to the vicinity of the specified value of 925 KEAS. Additional steps were then performed to approach a converged design.

As shown in Figure 3.3, the unbalanced-laminate final design had a structural weight of approximately 44.0 lb, or about 6.3 lb more than the starting fully stressed design. The detailed results indicated that this weight increment was associated almost entirely with the cover skins, and that approximately 7.5 lb had been added to achieve the increased flutter speed while about 1.2 lb had been removed due to the decreased stress levels resulting from strength/flutter interaction. The unbalanced-laminate layups for the

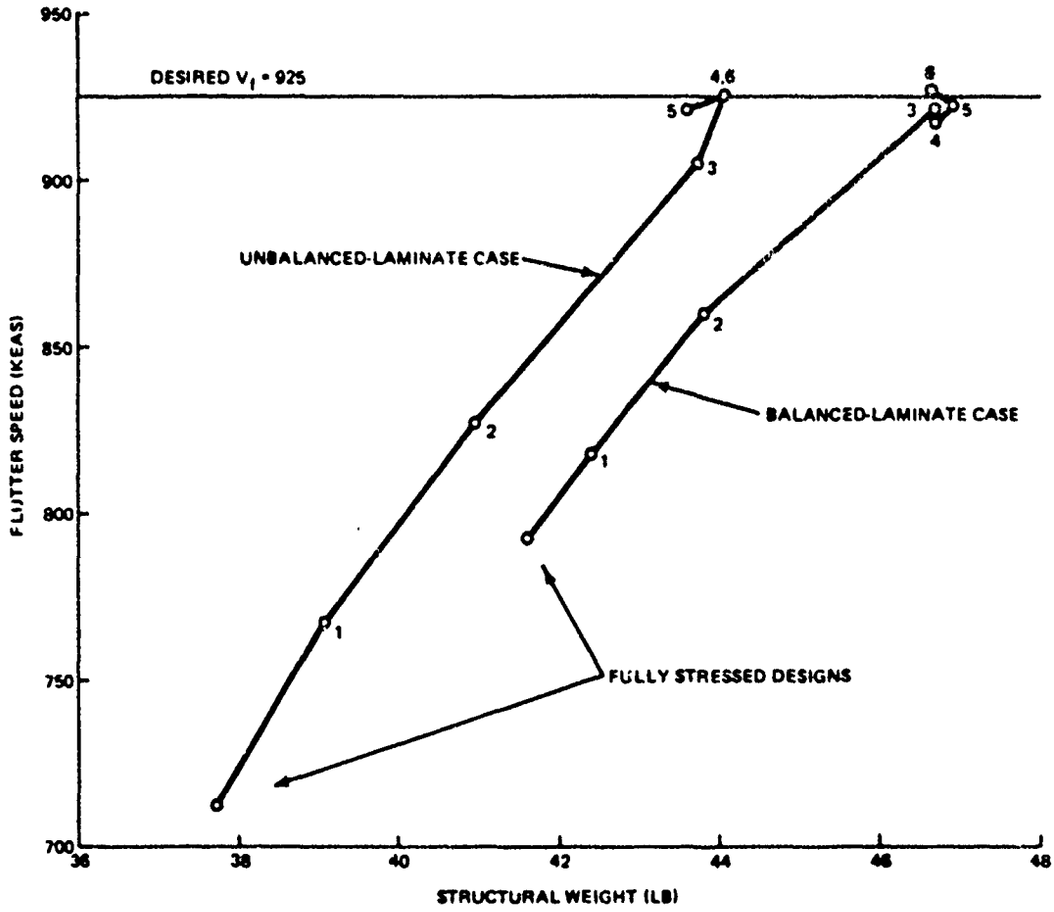

Figure 3.3 Strength/Flutter Redesign History for Intermediate-Complexity Wing

fully stressed design and for the final design are shown in Figure 3.4. Note the large increase in the thickness of the 0° layers in the trailing-edge panels near the root. The weight increase in this zone accounted for almost 70% of the total weight increment.

The results of the balanced-laminate redesign were qualitatively similar to the unbalanced case in that the weight increment was again primarily in the cover skins and involved a moderate amount of strength/flutter interaction. Figure 3.5 shows the balanced-laminate layups for the fully stressed design and the final design.

3.2.3 Results of Strength/Deflection Redesign Study

The deflection-constraint resizing study originally performed on the Intermediate-Complexity Wing to demonstrate the capability of the ASOP-3 program (Reference 4) has been repeated here to verify the same capability in FASTOP-3.

The fully stressed design for the unbalanced layup, discussed in the preceding subsection, was examined from the point of view of streamwise-twist distribution along the wing's span for the subsonic loading condition - the twist angle being based simply on the difference in vertical displacements between the forward and aft wing spars along a streamwise chord. This twist distribution is shown by the upper curve in Figure 3.6. It is interesting to note that the forward center of pressure of the subsonic loading distribution causes sufficient nose-up twisting to overpower the usual nose-down twisting (washout) that generally occurs in swept metallic wings.

To illustrate a potential application of the deflection-constraint resizing capability of FASTOP-3, it was decided to attempt to "tailor" the design to achieve a prescribed streamwise-twist distribution for the subsonic loading condition that would offer improved aerodynamic performance through increased lift-to-drag ratio. Twist angles at two wing stations were then established as targets, these being -2.0° (washout) at a selected inboard station and -2.5° at the most-outboard rib station (see Figures 3.1 and 3.6).

Resizing in the deflection-constraint mode was accomplished in two stages. The approach was to divide the structure in two regions, as indicated by the bold separating line in Figure 3.1. In the first resizing stage, only the composite cover skin elements in the inboard region were permitted to be

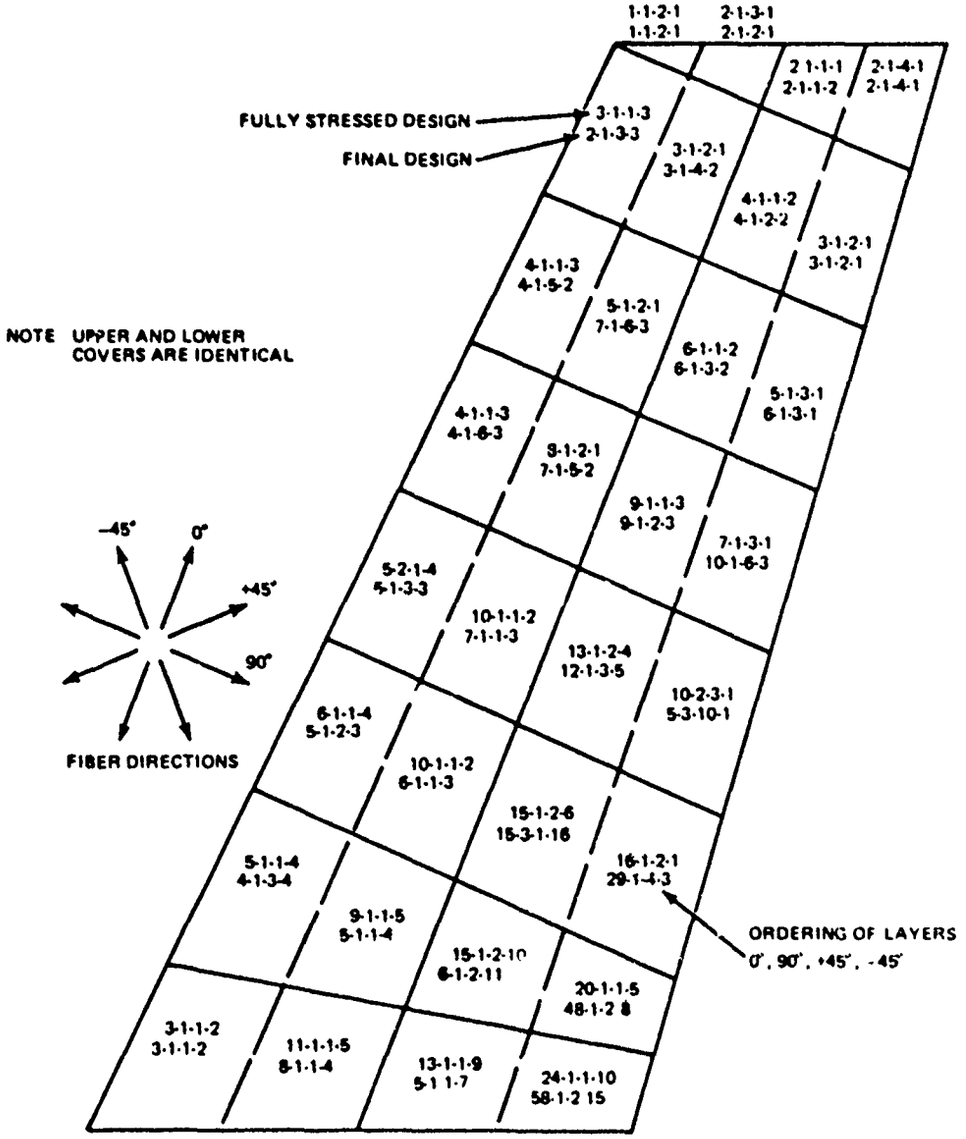

Figure 3.4 Cover-Skin Layups Following Strength/Flutter Resizing of Intermediate-Complexity Wing (Unbalanced-Laminate Case)

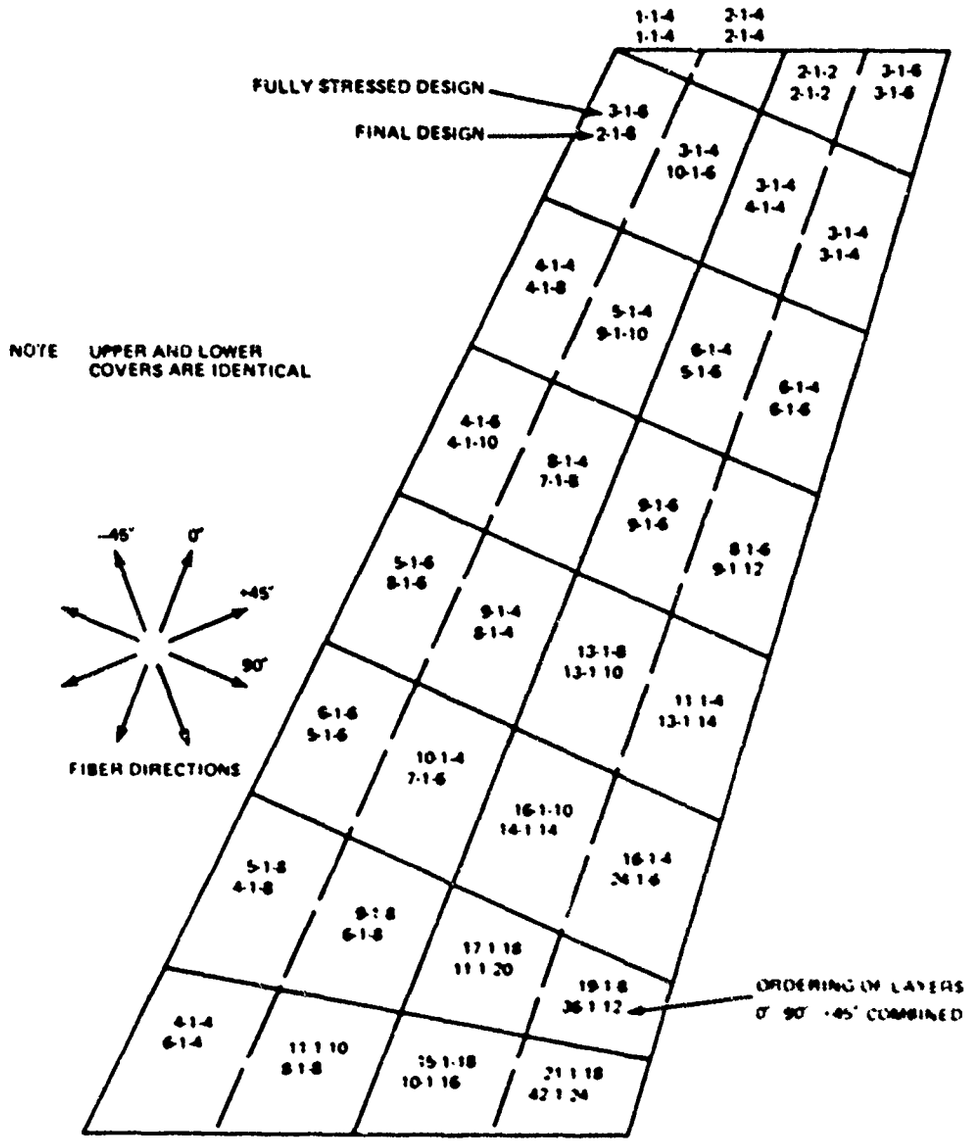

Figure 3.5 Cover Skin Layups Following Strength/Flutter Resizing of Intermediate-Complexity Wing (Balanced Laminate Case)

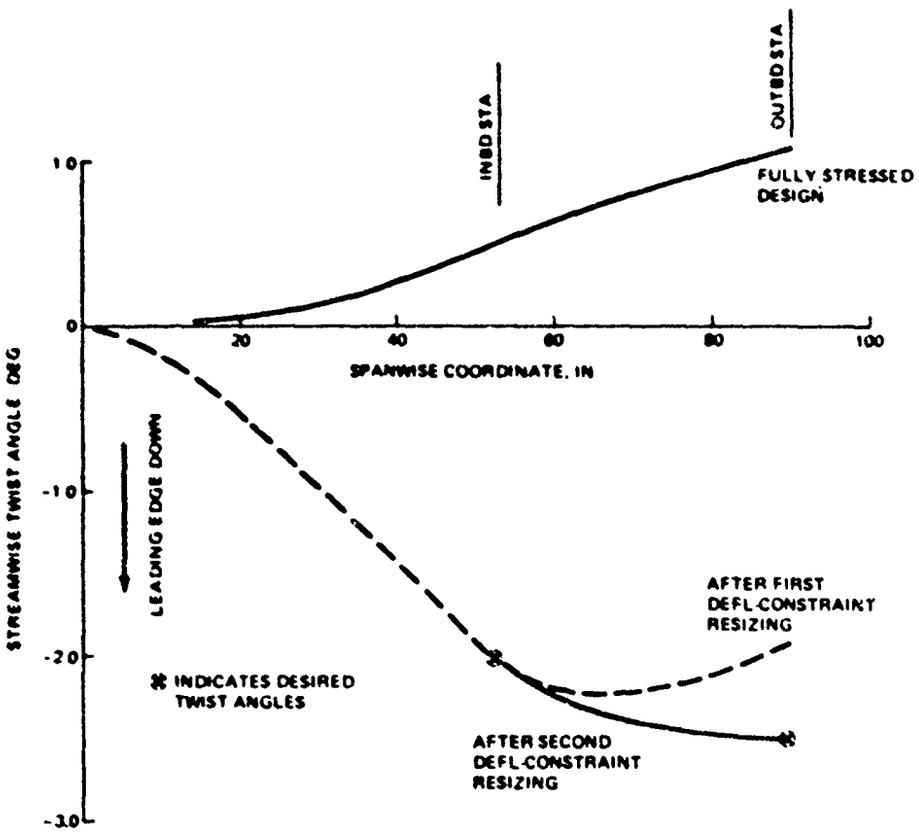

Figure 3.6 Intermediate-Complexity Wing – Streamwise Twist Distribution at Various Stages of Resizing for Deflection-Constraints

resized in the deflection part of a resizing cycle, to meet the inboard station twist-angle requirement. In the second stage, only outboard-region cover skin elements were allowed to be resized, to achieve the desired outboard-station twist angle. In both stages, however, all elements were permitted to be resized if they were strength critical. This two-stage approach was based on the concept that, for high-aspect-ratio cantilevered surfaces, the resizing of elements outboard of a particular station should have little influence on the deflections at that station.

The first stage of resizing in the deflection-constraint mode started with the fully stressed design. Convergence to the desired twist angle at the inboard station was achieved in eight steps, with the overall resulting twist distribution as shown by the dashed curve in Figure 3.6. Figure 3.7 summarizes the resizing history in this mode, in terms of inboard-station twist angle versus total structural weight, after the strength-resizing part of each cycle.

In the second stage of deflection-constraint resizing all starting gages were taken as those of the final design in the first stage. For elements in the inboard region, these starting gages were also treated as minimums, to prevent removal of material that was previously introduced to meet the inboard-station twist requirement. It should be noted that the introduction of these starting and minimum gages is fully automated in FASTOP-3 by making use of a stored member data file generated in the first resizing stage. This is different from ASOP-3, where considerable hand manipulation of member data is necessary.

Convergence to the desired outboard-station twist angle required only two cycles, with only a very small additional weight increase. The final twist distribution after this second deflection-constraint resizing is shown in Figure 3.6, and a summary of results for all stages of resizing is presented in Table 3.1. It should be pointed out that the small differences between the target and accepted twist angles are due mainly to limits imposed by the practical requirement for rounding layers to integral numbers of laminae. Figure 3.8 displays the wing cover layups for the initial fully stressed design and the final combined strength-and deflection-constrained design.

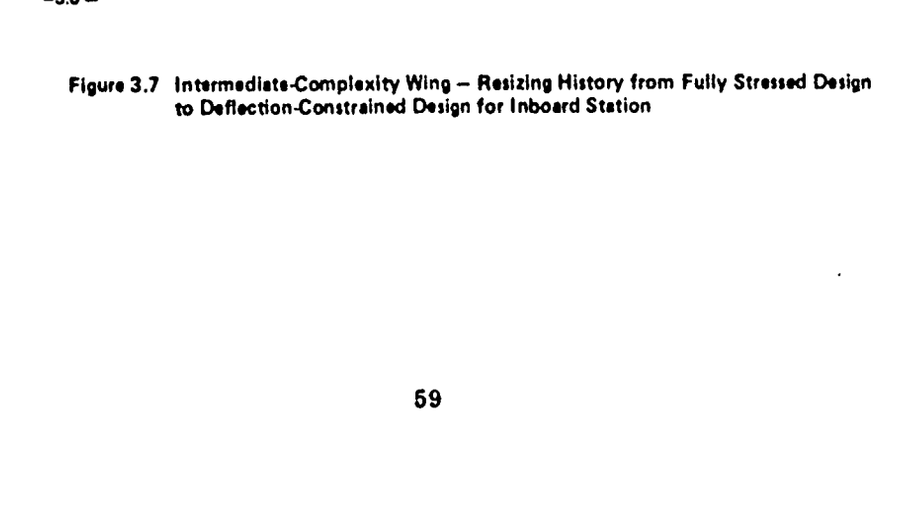

Figure 3.7 Intermediate-Complexity Wing – Resizing History from Fully Stressed Design to Deflection-Constrained Design for Inboard Station

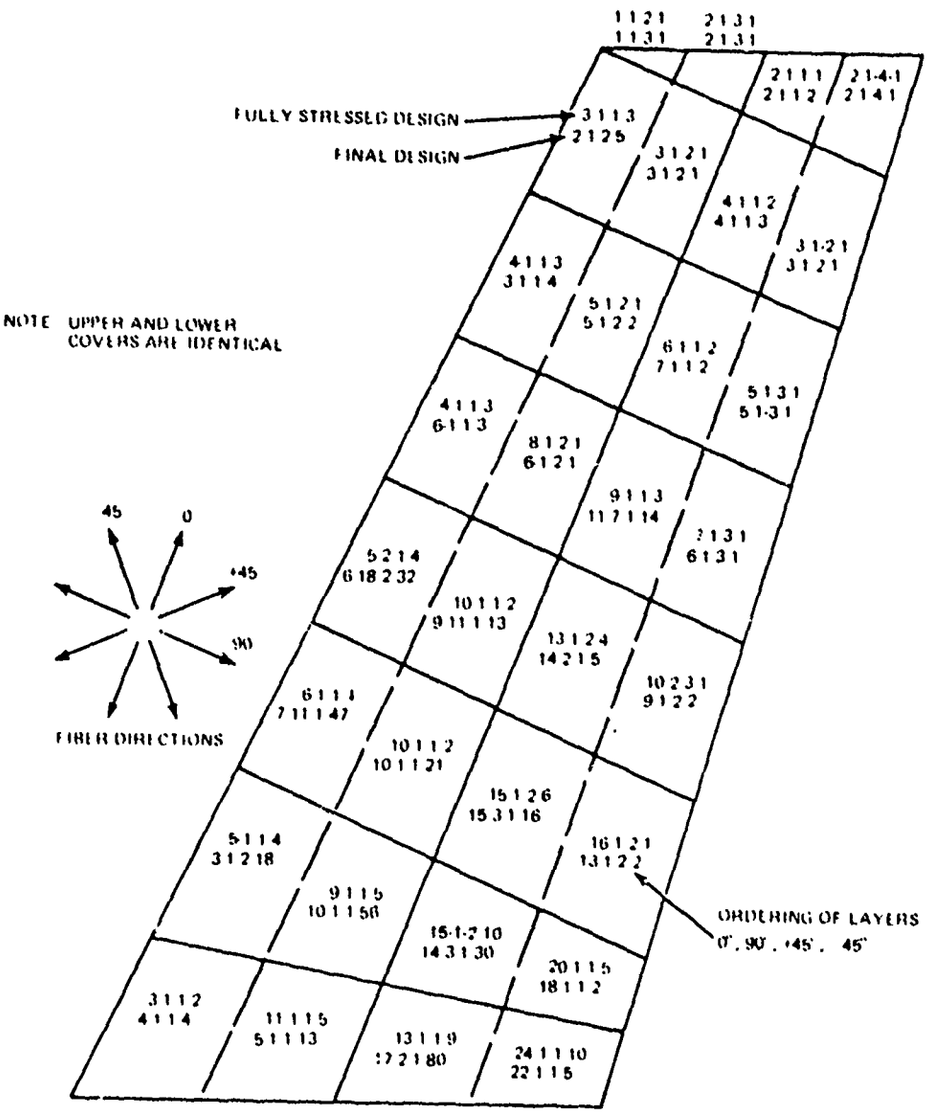

Figure 3.8 Cover-Skin Layups for Intermediate-Complexity Wing (Unbalanced-Laminate Case) Resized to Satisfy Strength and Deflection Constraints

TABLE 3.1. SUMMARY OF RESULTS FOR STRENGTH AND DEFLECTION-CONSTRAINT RESIZING OF INTERMEDIATE-COMPLEXITY WING

Constraint Mode	Cycles To Convergence	(1) θ Inbd	(2) θ Outbd	Structural Weight
Stress	5	+0.50°	+1.09°	37.7 lb
First Deflection	8	-2.01	-1.93	60.6
Second Deflection	2	-2.03	-2.51	61.2

(1) Desired Value = -2.00° (Leading Edge Down)

(2) Desired Value = -2.50° (Leading Edge Down)

3.3 ALL-MOVABLE STABILIZER

3.3.1 Mathematical Models

The aerodynamic planform and structural idealization of the all-movable stabilizer is shown in Figure 3.9. Cover skins, modeled as membrane elements, are of composite construction, except for small zones of metallic construction (the "splice-plates") in the vicinity of the support points. A hybrid laminate was selected to demonstrate the capability of the program. This laminate is constructed of boron/epoxy in the 0° (spanwise) direction, and graphite/epoxy in the ±45° and 90° directions. Titanium is used in the splice plate. The substructure, which is aluminum honeycomb material, is modeled as spanwise and ribwise shear panels having stiffness equivalent to the honeycomb. Posts are also present between upper- and lower-cover node points. In addition, there are metallic redistribution ribs and a few metallic spar webs in the vicinity of the splice plates. The details of the pivot restraints and the actuator arm are omitted from the figure to preserve clarity of presentation. It should be noted, however, that the inner and outer stabilizer-to-pivot supports are modeled in the mid-plane of the surface at points respectively enclosed by node-sets 481, 483, 463, 461 and 379, 381, 349, 347. In all, the model has 1172 degrees of freedom and 891 finite elements. Each cover has 162 members, all but 15 of which are composite elements requiring 4 design variables each.

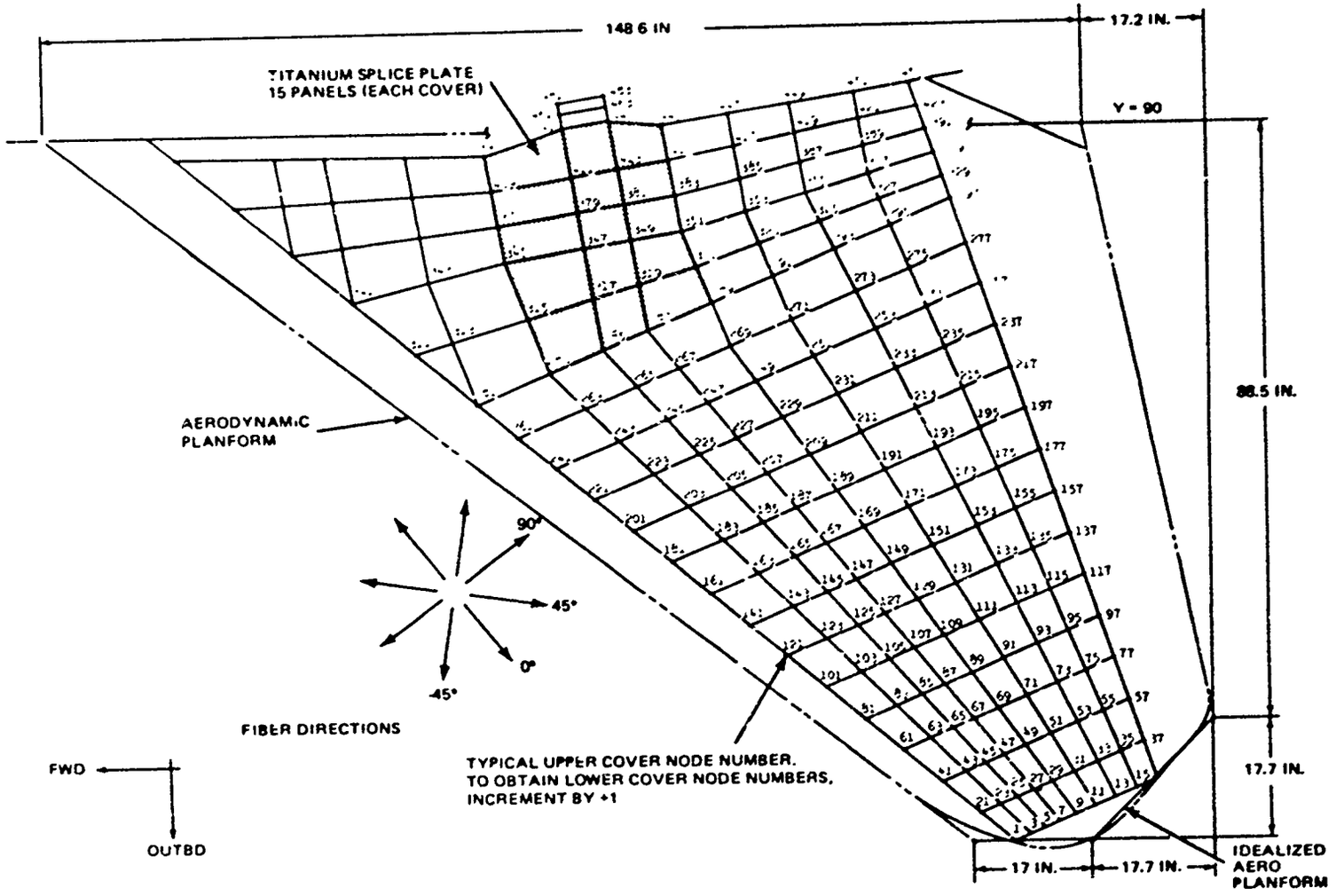

Figure 3.9 All-Movable Stabilizer Structures Model

Figure 3.10 shows the dynamics model of the all-movable stabilizer. Each of the 73 dynamics nodes lies in the mid-plane of the structure directly between upper- and lower-cover structural node points. Out-of-plane displacement is permitted at every dynamics node. In addition, to account for the effects of the overhung structure, 19 nodes along the front and rear spars have rotational degrees of freedom about either the front or rear spar directions. The model therefore has a total of 92 degrees of freedom.

3.3.2 Results of Strength/Flutter Redesign Study

In the redesign study of the all-movable stabilizer, resizing to satisfy both strength and flutter requirements was restricted to the elements in the cover skins only. All other elements in the structures model were effectively excluded from the entire redesign process because, for each of those elements, the minimum and maximum gages were set equal to the starting gage. As a result, the design problem involved 1206 active design variables, all but 30 of which were associated with the layers of the composite elements in the skins. The remaining 30 variables were associated with the metallic splice-plate elements.

For the stabilizer structures model described previously, fully stressed designs were obtained in 5 cycles for both the balanced- and unbalanced-laminate options; balancing was with respect to the ±45° layers. Three applied loading conditions were used, two of which (M = 0.8, S.L. and M = 1.3, 10,000 ft.) were generated within the automated load analysis module, ALAM. The unbalanced and balanced designs weighed 207 lb and 214 lb, respectively. Figure 3.11 shows the upper-cover layup of the unbalanced-laminate case. Note that all layers contain even numbers of laminae to enforce laminate designs having mid-plane symmetry. This feature was obtained by specifying double thicknesses for the laminae in the materials input data. Lower- and upper-cover layups were almost identical.

The Flutter Optimization Program (FOP) was then used to perform vibration analyses and Mach-box flutter analyses for both the unbalanced- and balanced-laminate fully stressed designs. Six normal modes of vibration were used in these flutter analyses which were done for a Mach number of 1.6 and an altitude of 30,000 feet. The resulting flutter speeds were 612 KEAS and 624 KEAS for the unbalanced- and balanced-laminate cases, respectively.

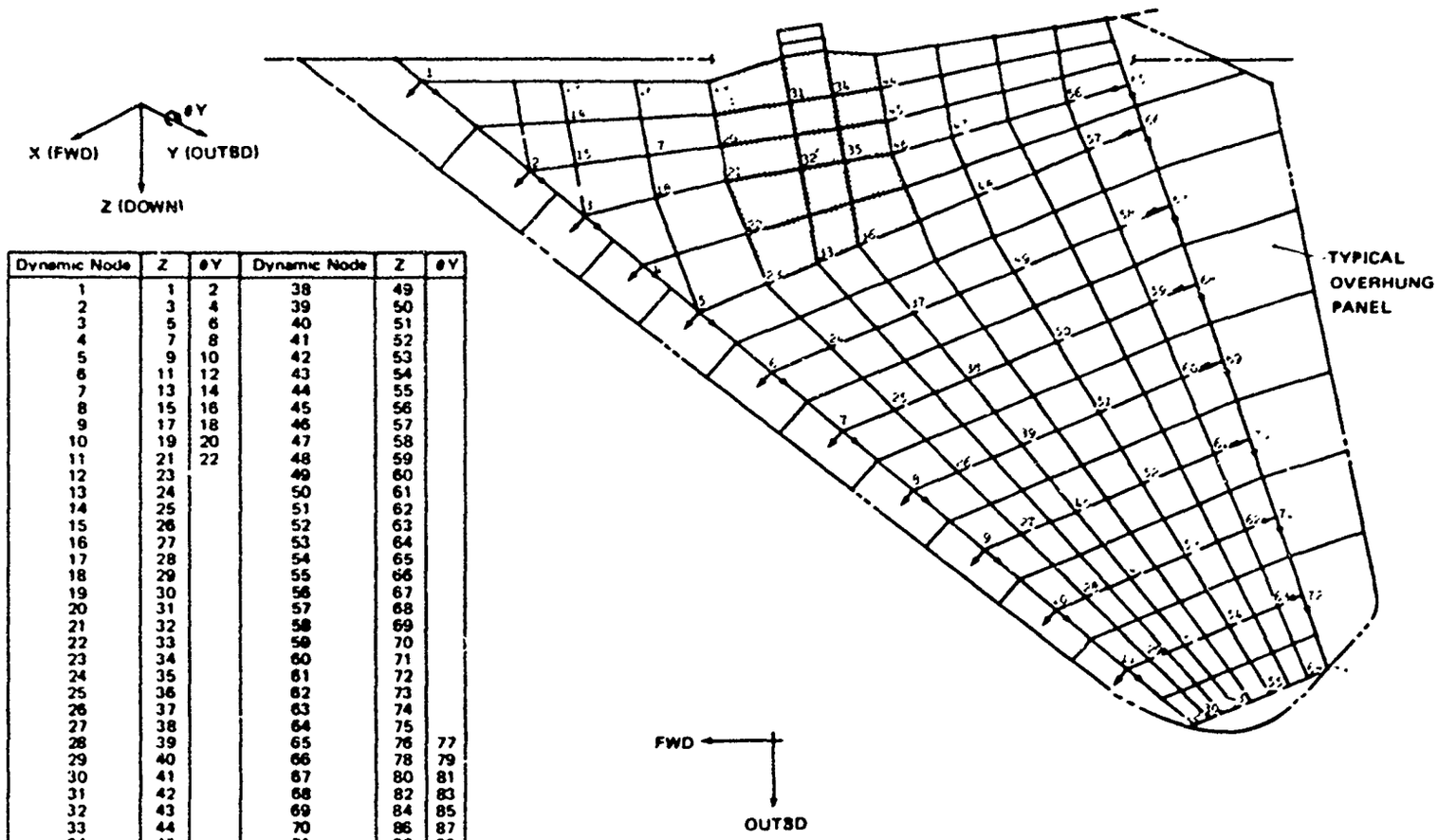

Dynamic Node	Z	θY	Dynamic Node	Z	θY
1	1	2	38	49	
2	3	4	39	50	
3	5	6	40	51	
4	7	8	41	52	
5	9	10	42	53	
6	11	12	43	54	
7	13	14	44	55	
8	15	16	45	56	
9	17	18	46	57	
10	19	20	47	58	
11	21	22	48	59	
12	23		49	60	
13	24		50	61	
14	25		51	62	
15	26		52	63	
16	27		53	64	
17	28		54	65	
18	29		55	66	
19	30		56	67	
20	31		57	68	
21	32		58	69	
22	33		59	70	
23	34		60	71	
24	35		61	72	
25	36		62	73	
26	37		63	74	
27	38		64	75	
28	39		65	76	77
29	40		66	78	79
30	41		67	80	81
31	42		68	82	83
32	43		69	84	85
33	44		70	86	87
34	45		71	88	89
35	46		72	90	91
36	47		73	92	
37	48				

Figure 3.10 All-Movable Stabilizer Dynamics Model

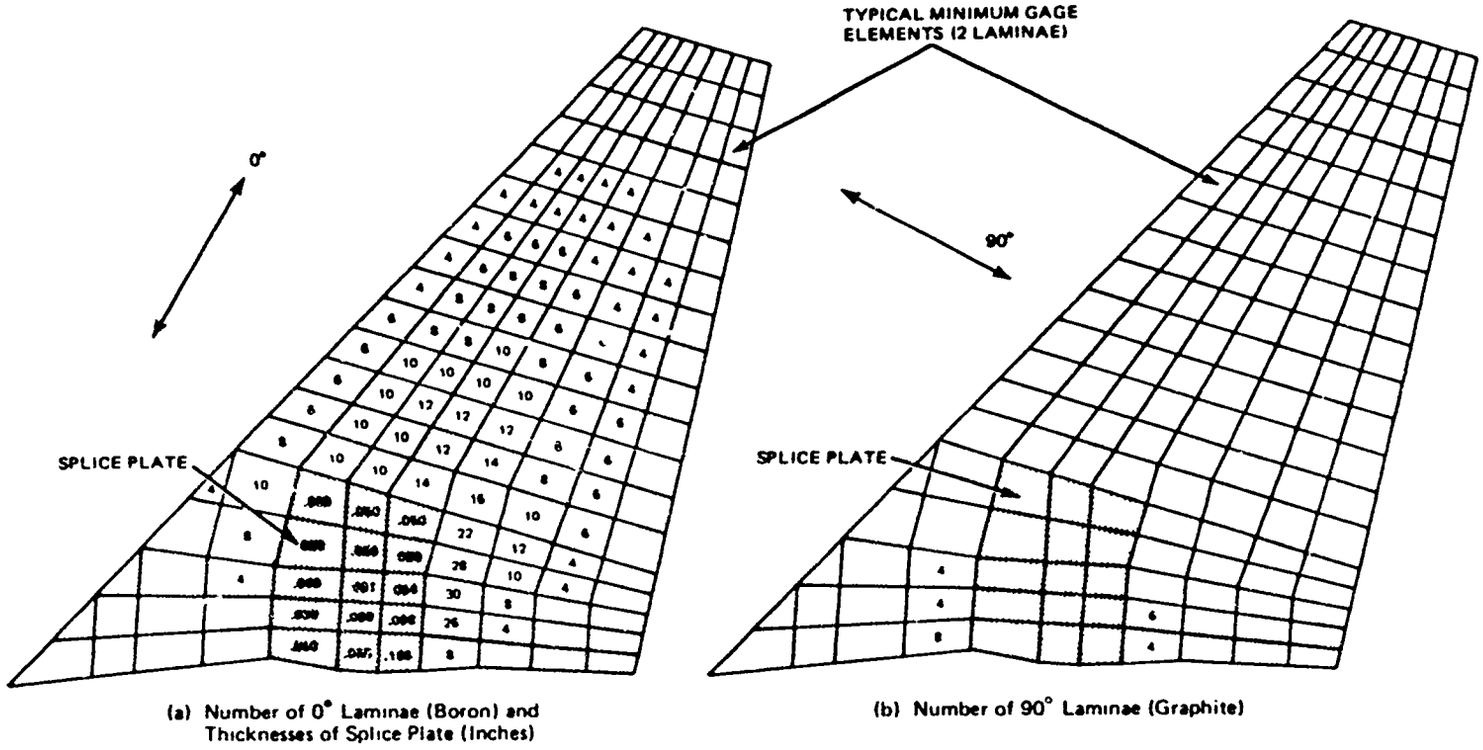

(a) Number of 0° Laminae (Boron) and Thicknesses of Splice Plate (Inches)

(b) Number of 90° Laminae (Graphite)

Figure 3.11 Stabilizer Upper Cover Unbalanced-Laminate Fully Stressed Design (Sheet 1 of 2)

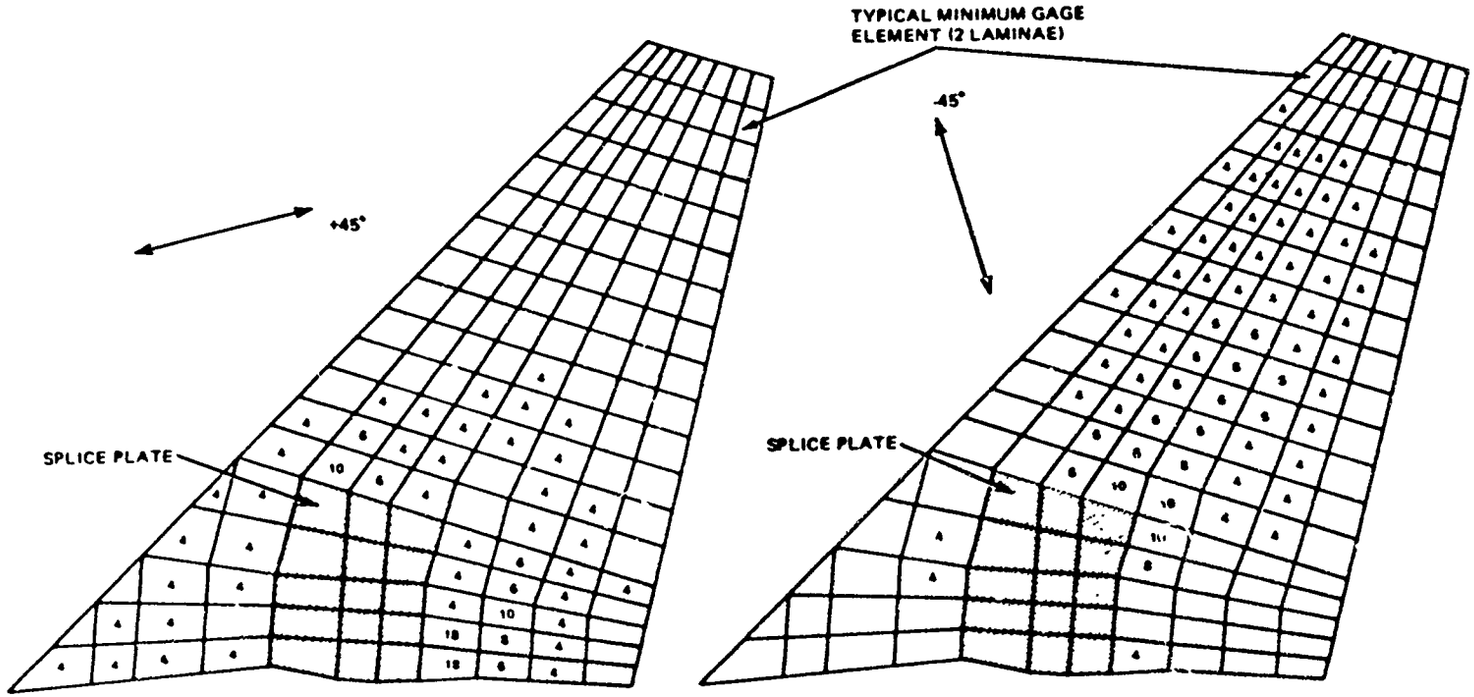

(c) Number of +45° Laminae (Graphite)

(d) Number of -45° Laminae (Graphite)

Figure 3.11 Stabilizer Upper Cover Unbalanced-Laminate Fully Stressed Design (Sheet 2 of 2)

Two parallel strength/flutter redesign studies were then performed to raise the flutter speeds of both designs to 765 KEAS (1.25 x 612). Figure 3.12 shows the history of the resizing steps. Note that a flutter speed close to the desired value was attained for each case in three combined resizing steps. Two additional steps were performed for the unbalanced case to approach a converged design.

The final design of the unbalanced-laminate case weighed 26 lb more than the fully stressed design from which it was derived. Approximately 40% of this weight increment went into the splice plates and the other 60% was distributed widely among the composite elements in various regions of the cover skins. Layers in all four fiber directions were affected. Figure 3.13 shows the unbalanced-laminate upper cover layup for the final design. A comparison of this layup with that of the fully stressed design (Figure 3.11) reveals several interesting points, which are discussed below.

First, significant amounts of material were added to the metallic splice plates and to the composite material in their vicinity. For the composite material, the numbers of 0° fibers aft of the plates and the +45° and 90° fibers forward of the plates (near the root rib) were increased.

Second, material was added in the middle third of the span to the -45° fibers and even more so to the +45° fibers.

Finally, material in all four fiber directions was added to the tip region, suggesting the presence of a mass-balance effect there, rather than a stiffness effect. Indeed, inspection of the fultter-velocity derivatives of the variables in that region showed that the derivatives were dominated by their kinetic-energy components, i.e., the strain-energy components were negligible. In an actual design effort, it would be more practical to group all the incremental tip material into a single mass-balance variable at the most favorable location, namely at the tip leading edge. Earlier flutter redesign studies on the metallic version of the stabilizer (see Reference 1) had shown that mass balance was extremely effective at the tip leading edge - so much so that a near-optimum design had been obtained with a single large mass at the tip and a relatively small amount of cover stiffening near the root rib in the vicinity of what is now the splice plates. This approach was not attempted in the current study because a final design of that type would neither test nor demonstrate the major new capability of FASTOP-3, namely strength/flutter

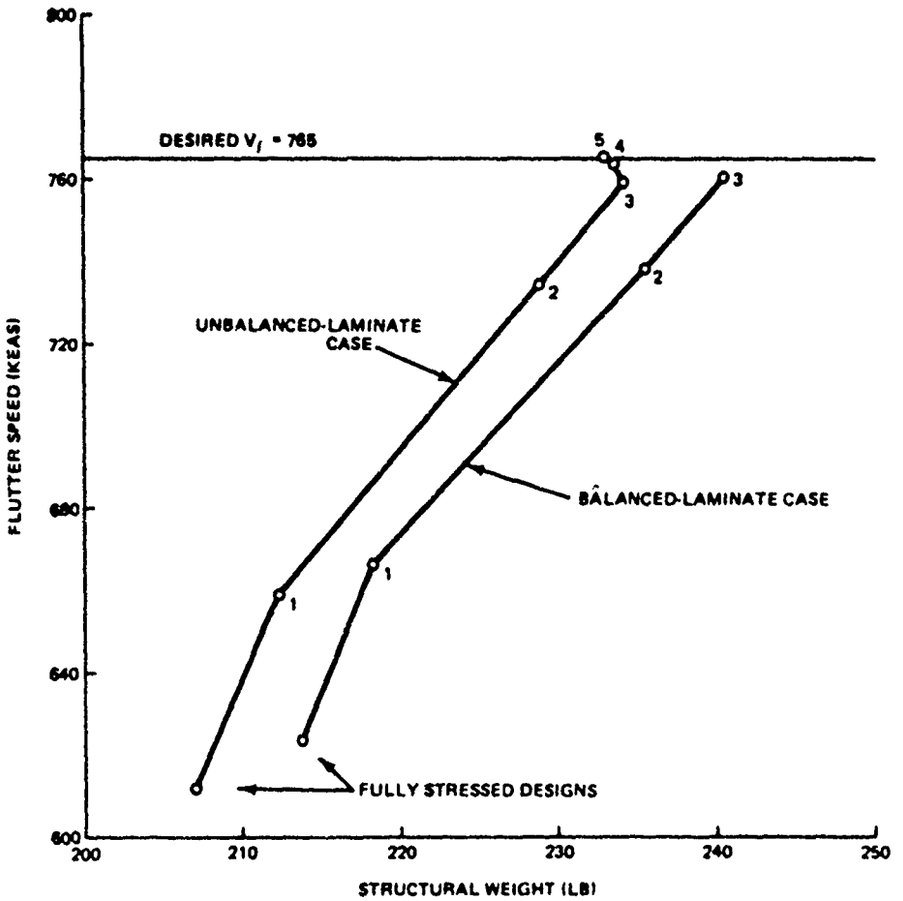

Figure 3.12 Strength/Flutter Redesign History for All-Moveble Stabilizer

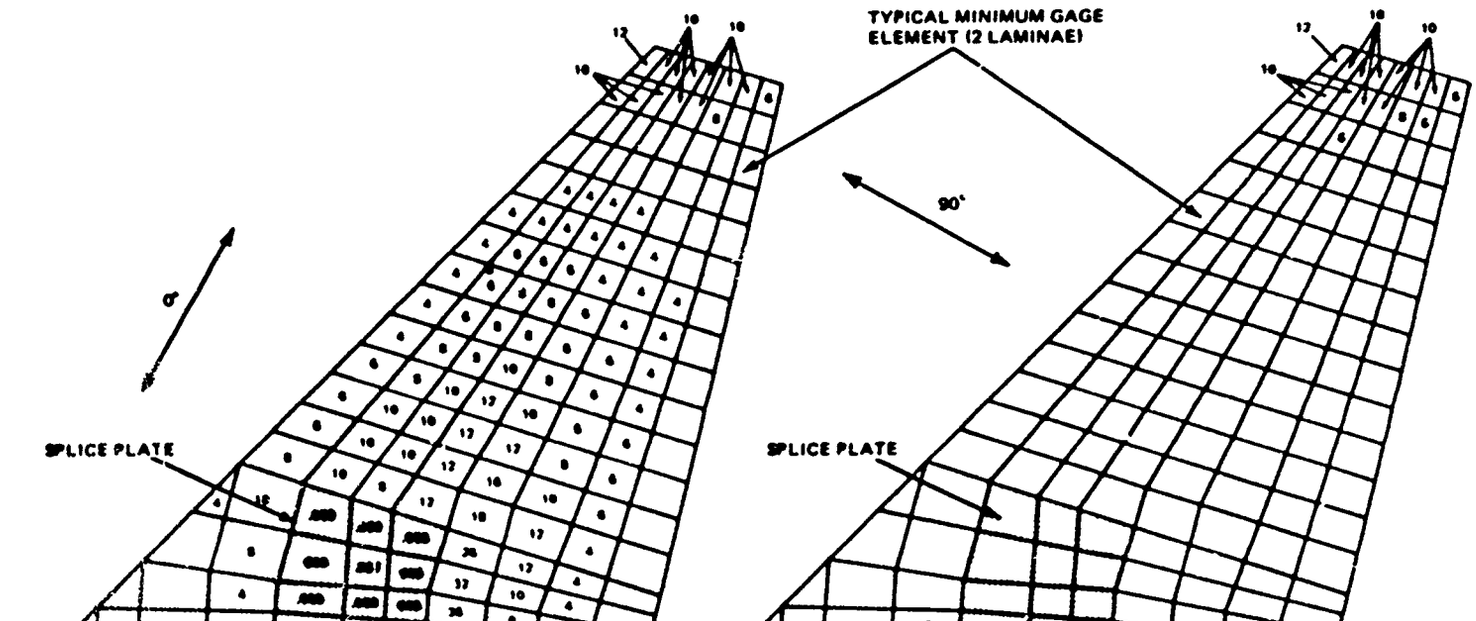

(a) Number of 0° Laminae (Boron) and Thicknesses of Splice Plate (Inches)

(b) Number of 90° Laminae (Graphite)

Figure 3.13 Stabilizer Upper Cover Unbalanced Laminate Final Design (Sheet 1 of 2)

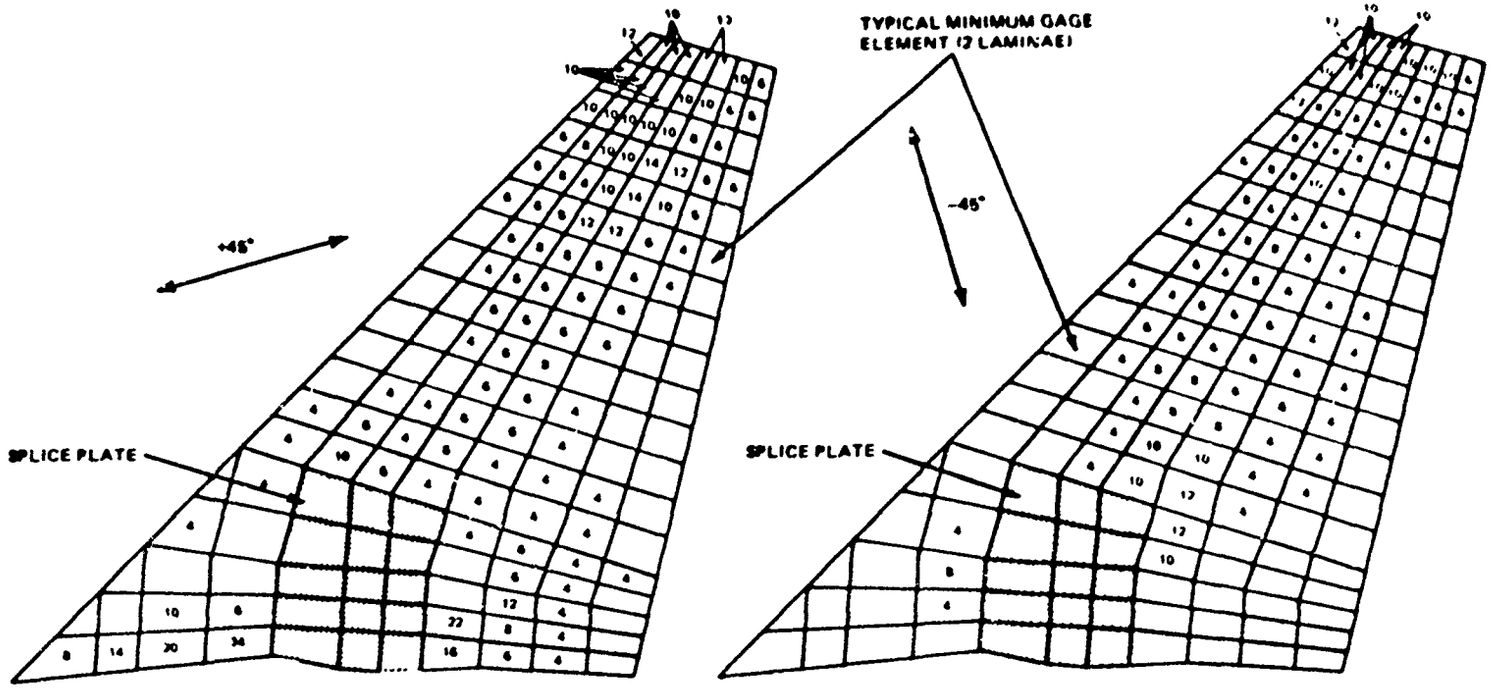

(c) Number of +45° Laminae (Graphite)

(d) Number of −45° Laminae (Graphite)

Figure 3.13 Stabilizer Upper Cover Unbalanced-Laminate Final Design (Sheet 2 of 2)

resizing of composite elements. It should be pointed out, however, that had several additional fultter resizing cycles been performed in the current study, it is likely that the program would have driven the design to one in which mass-balance was the dominant con'ributor to increased flutter speed.

REFERENCES

1. Wilkinson, K., Markowitz, J., Lerner, E., Chipman, R., George, D., et al. "An Automated Procedure For Flutter and Strength Analysis and Optimization of Aerospace Vehicles." Vol. I - Theory and Application. Vol. II - Program User's Manual, AFFDL-TR-75-137, December 1975.

2. Dwyer, W. J., Emerton, R. K., and Ojalvo, I. U., "An Automated Procedure for the Optimization of Practical Aerospace Structures. Vol. I - Theoretical Development and User's Information," Vol. II - Programmer's Manual, AFFDL-TR-70-118, April 1971.

3. Dwyer, W. J., "An Improved Automated Structural Optimization Program," AFFDL-TR-74-96, September 1974.

4. Isakson, G., and Pardo, H., "ASOP-3: A Program for the Minimum-Weight Design of Structures Subjected to Strength and Deflection Constraints," AFFDL-TR-76-157, December 1976.

5 Tsai, S. W., "Strength Characteristics of Composite Materials," NASA CR-224, April 1965, pp. 5-8

6. Sandhu, R. S., "A Survey of Failure Theories of Isotropic and Anisotropic Materials," AFFDL-TR-72-71, September 1972, pp. 19 and 22.

7. Jones, R. M., Mechanics of Composite Materials, Scripta Book Company, Washington, D. C., 1975.

8 Suarez, J A., Hadcock, R. N., and Whiteside, J. B., "The Influence of Local Failure Modes on the Compressive Strength of Boron-Epoxy Composites," Composite Materials: Testing and Design (Second Conference), American Society for Testing and Materials, ASTM STP 497, 1972, pp 237-256.

9. Lager, J. R., and June, R. R., "Compressive Strength of Boron-Epoxy Composites," J. Composite Materials, January 1969, pp, 48 56.

10 Zartarian, G., and Hsu, P. T., "Theoretical Studies on the Prediction of Unsteady Supersonic Airloads on Elastic Wings," Parts 1 and 2, WADC TR 56-97, February 1956.

REFERENCES

11. Pines, S., Dugundji, J., and Neuringer, J., "Aerodynamic Flutter Derivatives for a Flexible Wing with Supersonic and Subsonic Edges," Journal of the Aeronautical Sciences, Vol. 22, No. 5, May 1955, pp. 693-700.

12. Abramowitz, M., and Stegun, I. A., Handbook of Mathematical Functions with Formulas, Graphs and Mathematical Tables, National Bureau of Standards, Applied Mathematics Series 55, November 1964.

13. Evvard, J. C., "Distribution of Wave Drag and Lift in the Vicinity of Wing Tips at Supersonic Speed," NACA Technical Note 1382, July 1947.

14. Chipman, R. R., "An Improved Mach-Box Approach for the Calculation of Supersonic Oscillatory Pressure Distributions," Proceedings of the AIAA/ASME/SAE 17th Structures, Structural Dyanmics, and Materials Conference, King of Prussia, Pennsylvania, May 1976, pp. 615-621.

*U.S Government Printing Office: 1978 -- 757-080/696

SUPPLEMENTARY

INFORMATION

DEPARTMENT OF THE AIR FORCE

WRIGHT LABORATORY (AFMC)
WRIGHT-PATTERSON AIR FORCE BASE OHIO

ERRATA AD-B029162

1 Feb 96

MEMORANDUM FOR Defence Technical Information Center
8725 John J. Kingman Road, Suite 0944
Ft. Belvoir, VA 22060-6218

FROM: WL/DORT, Bldg 22
2690 C St Ste 4
Wright-Patterson AFB, OH 45433-7411

SUBJECT: Notice of Changes in Technical Report(s) AD B009874, AD B009781, AD B029162, AD B029330.
Please change subject report(s) as follows:

AFFDL-TR-75-137, Vol 1 (AD B009874): has been cleared for public release (State A).

AFFDL-TR-75-137, Vol II (ADB009781): has been cleared for public release (State A).

AFFDL-TR-78-50, Vol I (ADB029162): has been cleared for public release (State A).

AFFDL-tr-78-50, Vol II (ADB029330): has been cleared for public release (State A).

WL-TR-95-8014 (printed in Jan 95): Distribution statement should read as C - (B208214) Dist. authorized to US Gov Agencies and their contractors...

WL-TR-95-8015(printed in Jan 95): should read as Distribution Statement C - (B206558) Dist. authorized to US Gov agencies and their contractors....

ERRATA AD-B029162

Joseph A. Burke

JOSEPH A. BURKE, Team Leader
STINFO and Technical Editing
Technical Information Branch